S. Afr. J. Chem., 2019, **72**, 176–188,
<https://journals.sabinet.co.za/content/journal/chem/>.

Molecular Structure, FT-IR, NMR ($^{13}C/^{1}H$), UV–Vis Spectroscopy and DFT Calculations on (2Z, 5Z)-3-N(4-Methoxy phenyl)-2-N′(4-methoxy phenyl imino)-5-((E)-3-(2-nitrophenyl)allylidene) thiazolidin-4-one

Rachida Rahmani[a,b]§, Ahmed Djafri[a,c], Abdelkader Chouaih[a,*], Ayada Djafri[d], Fodil Hamzaoui[a,e] and Abdelghani M. Krallafa[f]

[a]*Laboratory of Technology and Solid Properties (LTPS), Abdelhamid Ibn Badis University – Mostaganem, 27000 Mostaganem, Algeria.*

[b]*Département de Génie des Procédés, Centre Universitaire Ahmed Zabana – Relizane, 48000 Relizane, Algeria.*

[c]*Centre de Recherche Scientifique et Technique en Analyses Physico-chimiques (CRAPC), BP 384-Bou-Ismail-RP 42004, Tipaza-Algeria.*

[d]*Laboratoire de Synthèse Organique Appliquée (LSOA), Département de Chimie, Faculté des Sciences, Université d'Oran 1 – Ahmed Ben Bella, 31000 Oran, Algeria.*

[e]*LPFM Académie de Montpellier, France.*

[f]*LCPM, Department of Chemistry, Faculty of Sciences, University of Oran 1, Ahmed Benbella, 31000, Algeria.*

Received 6 February 2019 Revised 9 July 2019 Accepted 9 July 2019.

ABSTRACT

In this study, some molecular properties of (2Z, 5Z)-3-N(4-methoxy phenyl)-2-N′(4-methoxy phenyl imino)-5-((E)-3-(2-nitrophenyl) allylidene) thiazolidin-4-one (MNTZ) are evaluated using a combination of spectroscopic characterization (FT-IR, ^{1}H and ^{13}C NMR chemical shifts) and theoretical calculations. Molecular geometry, vibrational wavenumbers, gauge-independent atomic orbital (GIAO), ^{1}H and ^{13}C chemical shift values and NBO analysis are investigated using B3LYP and PBE functionals with the 6-31G(d,p) basis set in the ground state. The calculated geometrical parameters and vibrational spectra are compared to available experimental data and each vibrational frequency is assigned on the basis of potential energy distribution (PED). The electronic transitions are calculated using time-dependent density functional theory (TDDFT). The energy band gap between the highest occupied molecular orbital (HOMO) and lowest unoccupied molecular orbital (LUMO) energies are obtained by computing the frontier molecular orbitals using the B3LYP/6-31G(d,p) and PBE/6-31G(d,p) levels along with the global reactivity descriptors. Mulliken atomic charges and molecular electrostatic potential (MEP) are simulated using both functionals to find more reactive sites for electrophilic and nucleophilic attack. Finally, the thermodynamic functions (heat capacity, entropy, and enthalpy) from spectroscopic data are obtained and discussed in the range of 100–1000 K.

KEYWORDS

FT-IR, UV-Vis, HOMO-LUMO, thiazolidinones, DFT, NMR spectra, NBO.

1. Introduction

It is well known that heterocyclic compounds are one of the most important classes of organic compounds. During the last few decades, they have attracted attention due to their proven usefulness in material sciences.[1–3] Moreover, the study of heterocyclic compounds is also of great interest theoretically. Specifically, thiazolidinones which belong to an important group of heterocyclic compounds, have been widely explored for their application in the field of medicine.[4,5] Thiazolidinones derivatives, particularly 4-thiazolidinones gained the attraction of researchers as a result of their broad-spectrum biological activity.[6–8] In addition, thiazolidinones are also known to exhibit push-pull effects and have photovoltaic applications due to the substituent at position 5 of the thiazole moiety.[9,10] On the other hand, the presence of heteroatoms nitrogen, oxygen or sulfur incorporated into the heterocyclic rings may have a strong effect on the polarity and polarizability of the molecule, the angle of rotation between its fragments, the planarity and thus on its stability.

In this paper, our interest was the thiazolidinones derivative, containing delocalized electrons. The π-conjugated system allows the title compound to exhibit the asymmetric electronic distribution which leads to increased charge transfer. Recently, the synthesis and X-ray crystal structure of the title compound was published.[11]

Based on these studies, and as a continuation of our previous work on thiazolidinone compounds[12–15], herein, we report the optimized molecular structure as well as a detailed spectroscopic study on (2Z, 5Z)-3-N(4-methoxy phenyl)-2-N′(4-methoxy phenyl imino)-5-((E)-3-(2-nitrophenyl) allylidene) thiazolidin-4-one (MNTZ) using IR, ^{1}H and ^{13}C NMR spectra. The natural bond orbital (NBO) analysis is carried out to interpret intra-molecular charge transfer (ICT). Besides considering charge transfer within this molecule, we have determined HOMO-LUMO orbitals and global reactivity descriptors. The reactivity and stability of MNTZ were determined by global chemical parameters such as ionization potential, the electron affinity, the absolute electronegativity, electrophilicity index, the absolute hardness and softness. The ionization potential represents the

* To whom correspondence should be addressed. E-mail: achouaih@gmail.com

ISSN 0379-4350 Online / ©2019 South African Chemical Institute / http://saci.co.za/journal
DOI: https://doi.org/10.17159/0379-4350/2019/v72a23

amount of energy required to remove an electron from an isolated atom or molecule where the electron affinity refers to the capability to accept one electron from a donor. These two parameters can be obtained from HOMO-LUMO analysis. The power of an atom in molecule to attract electrons to itself describes its electronegativity and the electrophilicity is defined as a measure of the propensity of a species to accept electrons. The electrophilicity index was calculated using the electronic chemical potential and chemical hardness. A good, more reactive, nucleophile is characterized by a lower value of chemical potential and electrophilicity index, and conversely a good electrophile is characterized by a high value of chemical potential and electrophilicity index. The UV-Visible spectroscopic studies along with the calculated value of the band-gap energy were used to interpret charge transfer within the molecule. Mulliken population analysis, molecular electrostatic potential (MEP) and thermodynamic parameters were investigated using B3LYP and PBE functionals in the gas phase.

2. Experimental and Computational Details

Synthesis, solid state structure and spectral data (IR, ^{1}H NMR, ^{13}C NMR) of the title compound are reported in our previous work.[11] IR spectra were recorded in KBr pellet on a JASCO FT/IR 4210 Fourier Transform Infrared Spectrometer and the reported wave numbers were given in cm^{-1}. The ^{1}H NMR and ^{13}C NMR were recorded on Brüker Ac DPX-200(300 MHz) spectrometer in $CDCl_3$ as solvent using tetramethylsilane as an internal reference standard.

Density functional theory (DFT) has proved to be extremely useful for studying the electronic structures of molecules. Calculations of the new (2Z, 5Z)-3-N′(4-methoxy phenyl)-2-N′(4-methoxy phenyl imino)-5-((E)-3-(2-nitrophenyl) allylidene) thiazolidin-4-one (MNTZ) are carried out using the Gaussian 09 program and GaussView molecular visualization software.[16,17] The parent structure for the calculations is obtained from the X-ray coordinates[11] and this structure is optimized at the DFT level of theory with the B3LYP[18,19] and PBE[20] functionals and the 6-31g(d, p) basis set. Optimized structures are used in the vibrational frequency calculations to ensure that the obtained structures represent a local minima. The theoretical vibrational spectrum is interpreted through the Potential Energy Distribution (PED) using Vibrational Energy Distribution Analysis (VEDA) program.[21] The nuclear magnetic resonance (NMR) chemical shift calculations are undertaken using the Gauge-Independent Atomic Orbital (GIAO) method at B3LYP/6-31G(d,p) level. Chloroform solvent effects on theoretical NMR parameters were included using single point calculation on optimized gas phase geometry.

The time-dependent density functional theory (TD-DFT) method on the ground state was used to calculate the excited states and the electronic transitions. The chloroform solvent effect has been considered using the Polarized Continuum Model (PCM).[22] The vertical transition wavelength/energies are calculated for 10 excited singlet states by the TD-DFT methodology using the same functionals as geometry optimization. The NBO analysis is performed with DFT/B3LYP/6-31g(d,p) level to elucidate the conjugation, charge transfer and delocalization of electron density within the molecule. Besides, Mulliken and NBO atomic charges, the molecular electrostatic potential (MEP), frontier molecular orbital (FMOs), the dipole moment and thermodynamic properties of MNTZ were investigated using both functionals.

3. Results and Discussion

3.1. Optimized Geometry

The optimized structure of MNTZ molecule is given in Fig. 1 with atomic labelling and the corresponding cartesian/internal coordinates are reported in Table S1 (see supplementary information). The geometrical parameters (bond lengths, bond angles, and dihedral angles) computed by B3LYP and PBE functionals with the 6-31G(d,p) basis sets are listed in Tables S2, S3 and S4 (see supplementary information), together with the X-ray parameters.[11] The differences between calculated and experimental bond lengths and angles are within a few Angstroms and degrees, respectively, when compared to the experimental parameters, which indicate that our calculations are acceptable. The small differences can be due to the fact that calculated data are collected in the gas phase, while the experimental data are acquired in the solid state.

To get a better comparison of the geometrical parameters, correlation graphs between the calculated and the experimental parameters of bond lengths, bond angles and dihedral angles are shown in Fig. 2, Fig. 3 and Fig. 4, respectively. The correlation

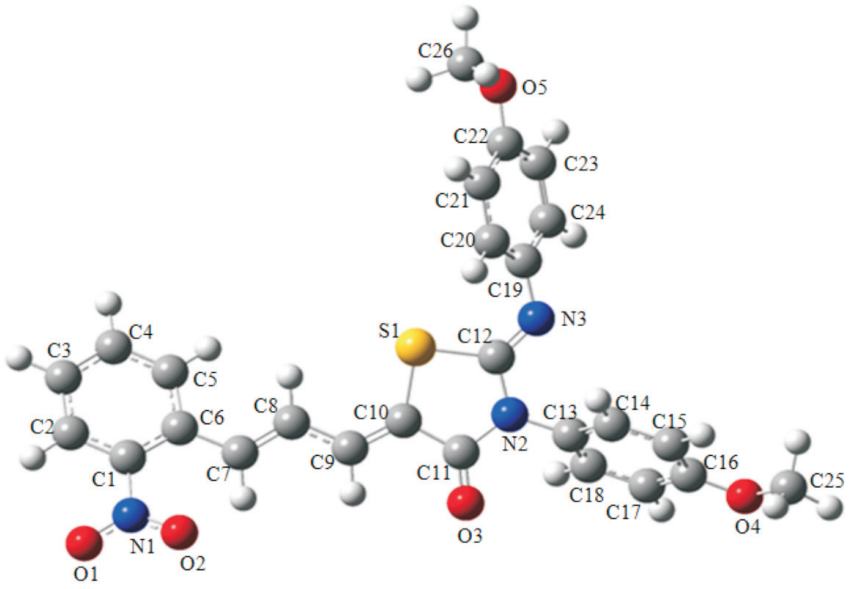

Figure 1 Optimized geometry with the atomic numbering scheme of MNTZ obtained from the B3LYP level.

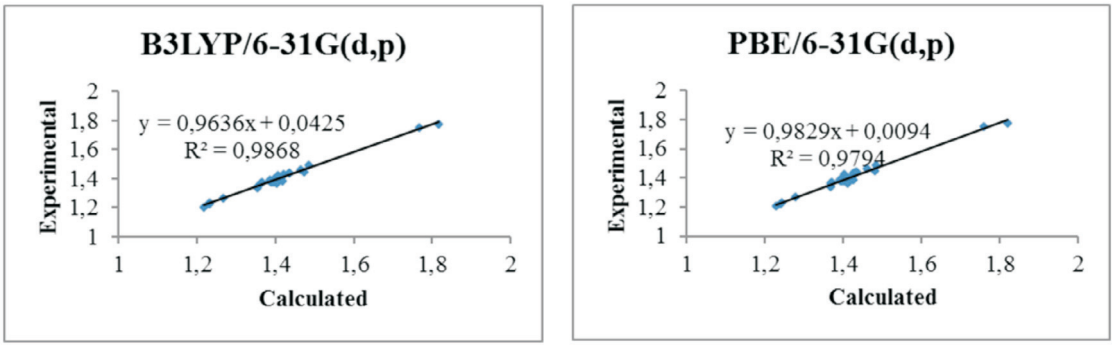

Figure 2 Correlation graphics of calculated and experimental bond lengths of MNTZ.

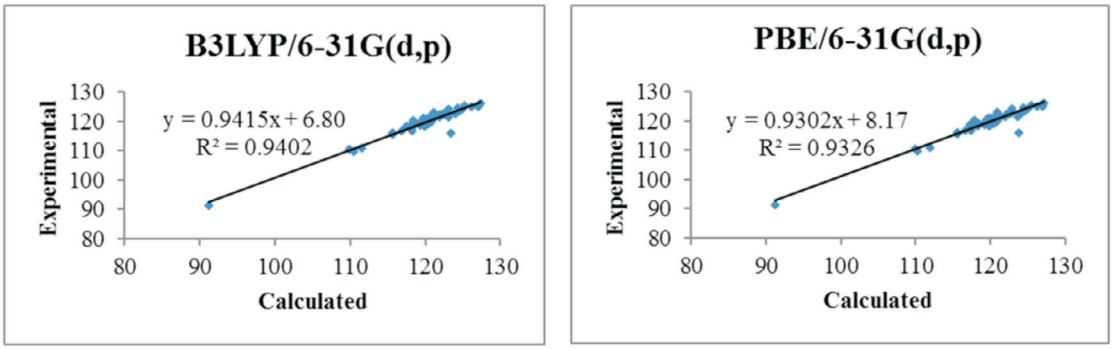

Figure 3 Correlation graphics of calculated and experimental bond angles of MNTZ.

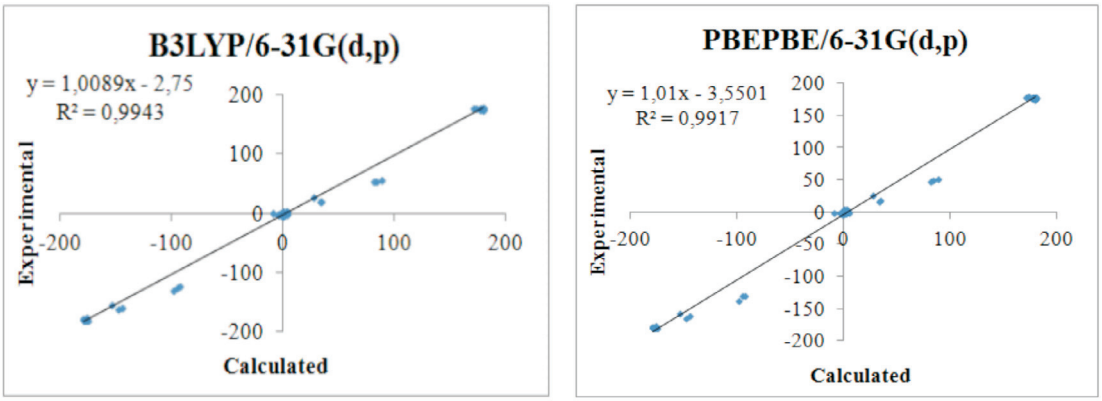

Figure 4 Correlation graphics of calculated and experimental dihedral angles of MNTZ.

values R^2 obtained by B3LYP and PBE functionals with 6-31g(d,p) basis set are 0.9868 and 0.9794 for bond lengths, 0.9402 and 0.9326 for bond angles and 0.9943 and 0.9917 for dihedral angles. These results confirmed the good agreement between calculated and experimental parameters.

3.2. Vibrational Assignments

The experimental FT-IR and the calculated wavenumbers by B3LYP and PBE methods with 6-31g(d,p) basis set and their assignment using potential energy distribution (PED) calculation are given in Table S5 (see supplementary information). The calculated and experimental infrared spectra are shown in Fig. 5. No imaginary frequency has been found, which means that the optimized geometry is located at the local lowest point on the potential energy surface. The calculated frequencies are higher than the experimental values for the majority of the normal modes, for this reason, the scaling factors 0.961 and 0.986 are used for B3LYP and PBE calculated frequencies[23,24], respectively. The MNTZ consists of 56 atoms and hence it shows 162 (3N-6) normal modes of vibration[25] active in infrared absorption.

3.2.1. *C-H Vibrations*

The C–H stretching vibrations of aromatic compounds appear in the range of 3100–3000 cm^{-1}.[26] In the present study, the phenyl ring CH stretching vibrations are predicted at the region 3120–3070 cm^{-1} for B3LYP and 3128–3084 cm^{-1} for PBE, which are in good agreement with the observed value of 3057.7 and 3008.8 cm^{-1} in FT-IR spectrum.

The experimental wavenumbers of CH stretching vibrations of allylidene fragment are observed at 2951 and 2930 cm^{-1} in the FT-IR spectrum. The corresponding theoretical values are 3058–3039 cm^{-1} for B3LYP and 3064–3048 cm^{-1} for PBEPBE functional.

The in-plane C–H bending vibration occurs in the region 1300–1000 cm^{-1}.[27] This vibration is computed in the range 1460–985 cm^{-1} for B3LYP and 1448–978 cm^{-1} for PBE and the corresponding experimental values are found in the region 1296–1009 cm^{-1} in FT-IR. The out-of-plane C–H bending vibrations give rise to bands in the region 900–625 cm^{-1}.[28] This vibration is predicted at 967–520 and 950–512 cm^{-1} with B3LYP and PBE levels, respectively, and observed at 968–647 cm^{-1} in FT-IR.

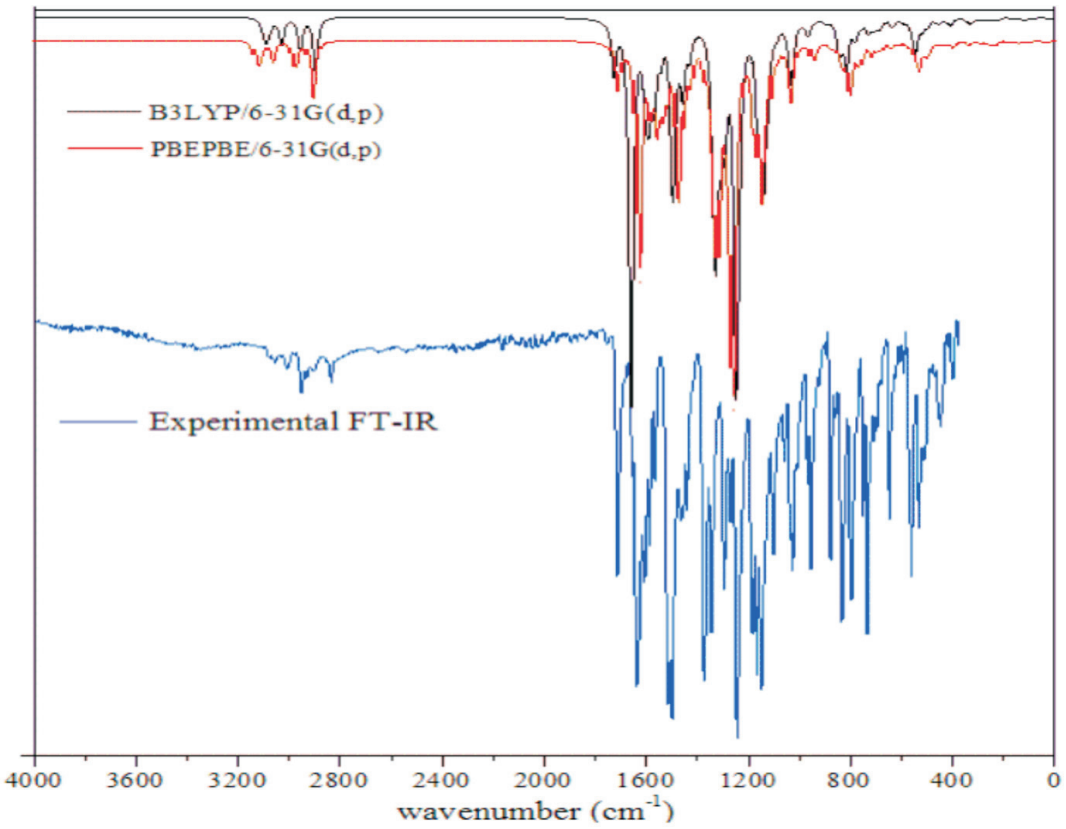

Figure 5 The experimental FT-IR and theoretical IR spectra of MNTZ.

3.2.2. *C=C Vibrations*

Generally, the C=C stretching vibrations in aromatic compounds occur in the region 1650-1430 cm^{-1}.[29] In the present study, the C=C stretching vibration of benzene rings appears at 1637, 1608, 1513.7 and 1439.8 cm^{-1} in the FT-IR spectrum. The corresponding computed values are 1609, 1542 and 1423 cm^{-1} for ring 1 (C1–C6), 1605, 1573 and 1409 cm^{-1} for ring 2 (C13–C18) and 1601, 1557 and 1404 cm^{-1} for ring 3 (C19–C24). On the other hand, the band observed at 1587 cm^{-1} in the FT-IR spectrum is assigned to C=C stretching vibration of allylidene fragment. The corresponding predicted values with the B3LYP level are 1593 and 1583 cm^{-1} for C7=C8 and C9=C10, respectively.

3.2.3. *C=N Vibration*

The observed frequency at 1654 cm^{-1} in the infrared spectrum is assigned to C=N stretching vibrations. This vibration appears at 1658 cm^{-1} in theoretical IR computed with B3LYP/6-31g(d,p) level and shows a pure mode and its PED contribution is about 74 %.

3.2.4. *Nitro Group Vibrations*

The asymmetrical stretching vibrations of substituted nitrobenzene occur in the region 1560–1490 cm^{-1},[30] and symmetric stretching vibrations occur in the region 1370–1310 cm^{-1}. The FT-IR spectrum for MNTZ gives peaks at 1566.1 and 1374.4 cm^{-1}, and these peaks are assigned as asymmetric and symmetric NO_2 stretching vibrations. These peaks are predicted at 1566 and 1339 cm^{-1} for B3LYP and 1551, 1353 cm^{-1} for PBE, respectively. The asymmetric NO_2 stretching vibration calculated by B3LYP is found to be exactly correlated with the experimental one. The observed NO_2 in-plane bending vibration is assigned at 841cm^{-1} in the FT-IR spectrum. The wavenumbers are computed at 842 and 814 cm^{-1} for the scissoring modes which are correlated with the experimental values. Furthermore, the out-of-plane bending vibration is observed at 683 in the FT-IR spectrum. The corresponding calculated values are 771 and 682 cm^{-1} with the B3LYP level.

3.2.5. *Methoxy Group Vibrations*

The asymmetric and symmetric CH stretching vibrations of the two methyl groups occur in the region 3029–2954 and 2900–2896 cm^{-1} for B3LYP/6-31g(d,p) level, respectively. These vibrations are observed at 2930–2834 cm^{-1} in the FT-IR spectrum. The in-plane bending modes of CH_3 appear at 1461 cm^{-1} in the FT-IR spectrum. The calculated values at 1460 and 1430 cm^{-1} obtained by B3LYP level are consistent with FT-IR results. Moreover, the out-of-plane bending vibrations are measured at 1166 in FT-IR and computed at 1165 and 1133 cm^{-1} with B3LYP/6-31g(d,p). The bands calculated in the range 1036–1035, 280–227 and 156–85 cm^{-1} are assigned as the stretching O-C, in-plane and out of plane C-OCH_3 vibrations.

3.2.6. *Thiazolidinone Group Vibrations*

Vibrational analysis of thiazolidinone group is made on the basis of C=O, C-N, and C-S vibrations. The carbonyl stretching vibration is observed at 1713 cm^{-1} in the experimental infrared spectrum and calculated at 1725 and 1711 cm^{-1} with B3LYP and PBE levels, respectively. The stretching C-N vibration gives rise to a band at 1345 cm^{-1} in the FT-IR spectrum and the corresponding calculated values are 1327 and 1351 cm^{-1} with B3LYP and PBEPBE levels, respectively. The bands observed at 591 and 446.9 cm^{-1} in the IR spectrum are assigned to stretching νC-S and bending δCSC, respectively. These bands are calculated at 588 and 446 cm^{-1} with the B3LYP level. All these results are in good agreement with the literature.[31–33]

3.3. ^{1}H and ^{13}C NMR Spectral Analysis

The theoretical ^{1}H and ^{13}C NMR isotropic shielding were com-

puted with the B3LYP/ 6-31G(d,p) level using chloroform as a solvent and the gauge-independent atomic orbital (GIAO) method.[34] The TMS shieldings with B3LYP/GIAO/6-31G(d,p) are 31.74 ppm and 192.12 ppm for ^{1}H and ^{13}C NMR, respectively.[35] The chemical shift of the studied molecule is $\delta_{(MNTZ)}$ where $\delta_{(MNTZ)} = \sigma_{(TMS)} - \sigma_{(MNTZ)}$ (σ is a chemical shielding).[36] ^{1}H and ^{13}C NMR spectra of MNTZ are shown in Fig. 6 and Fig. 7, respectively. The experimental and calculated ^{1}H and ^{13}C isotropic chemical shifts for MNTZ using the B3LYP/6–31G(d,p) level of theory are given in Table S6 (see supplementary information).

The ^{1}H NMR spectrum (Fig. 6a) of MNTZ in chloroform shows two singlet peaks at 3.81 and 3.85 ppm for the methoxy moieties, the corresponding calculated ranges (Fig. 6b) are 3.58–3.95 ppm for $O_{25}CH_3$ and 3.61–3.97 ppm for $O_{26}CH_3$. The aromatic ring protons give signals in the range of 6.9–8 ppm. The singlet peak at 8 ppm is assigned to the H2 proton (calculated value as 8.4 ppm). Also, the singlet peak at 6.9 ppm is assigned to phenyl protons (H15, H17, H21, and H23), the corresponding calculated values are 7.0, 6.8, 6.9 and 6.8 ppm, respectively. The doublet peak at 7.04 ppm is assigned to H20 and H24 protons and the doublet peak at 7.35 ppm is assigned to H14 and H18 protons which correlated with the calculated value of 7.4 ppm. The multiplet between 7.43–7.67 ppm is assigned to H3, H4 and H5 protons. For the allylidene fragment protons, H8 appears as a

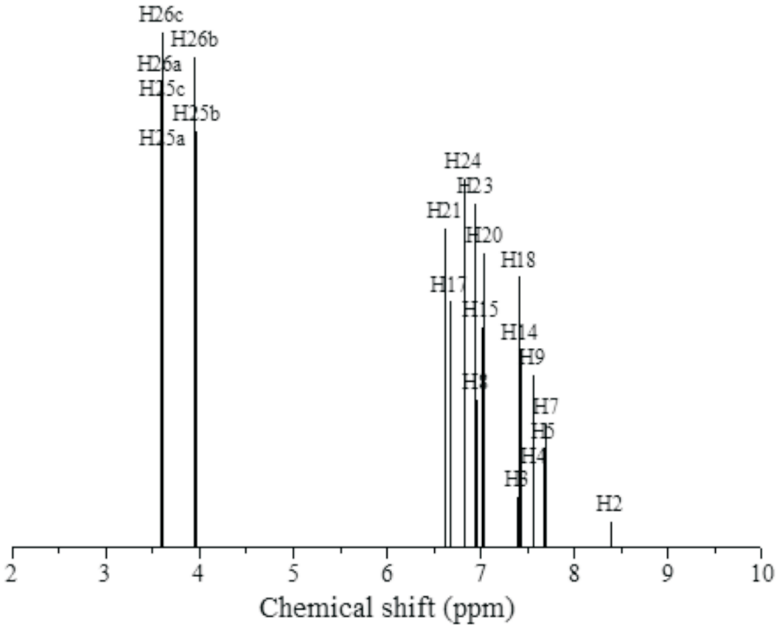

(a)

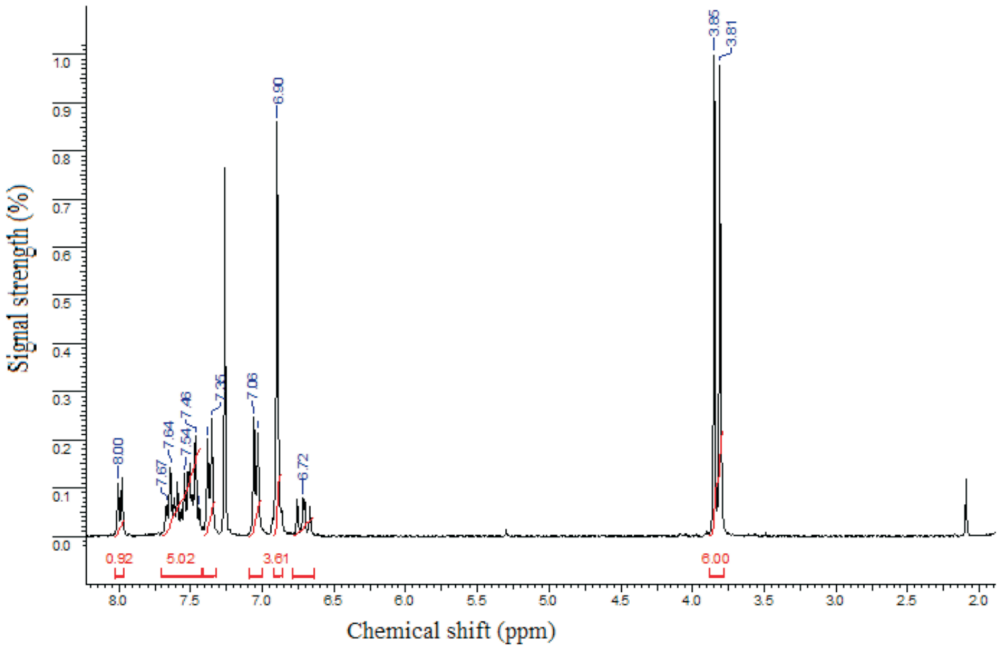

(b)

Figure 6 (**a**) ^{1}H NMR chemical shift and (**b**) calculated ^{1}H NMR for MNTZ.

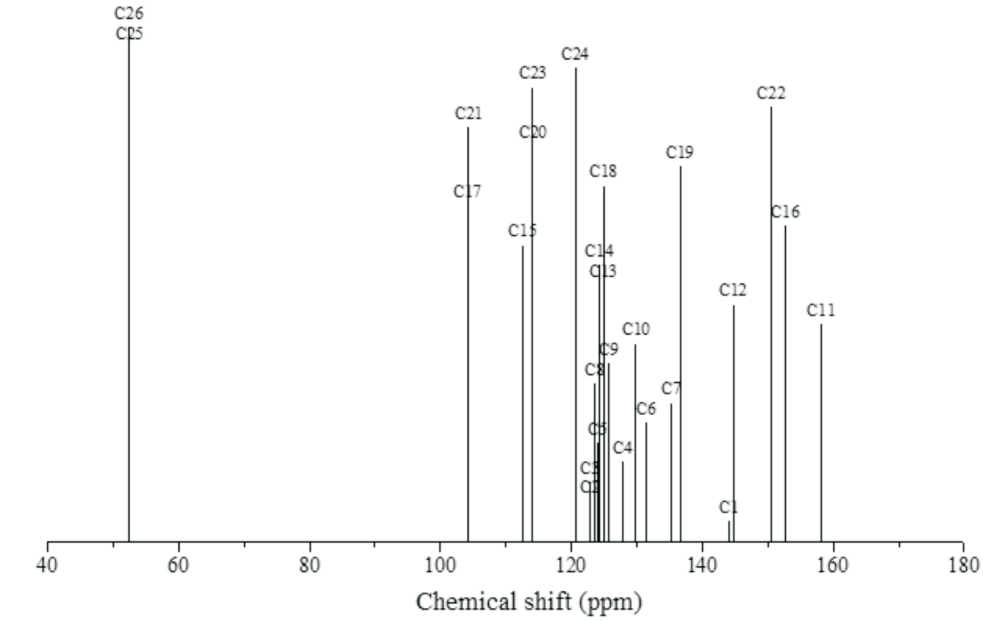

(a)

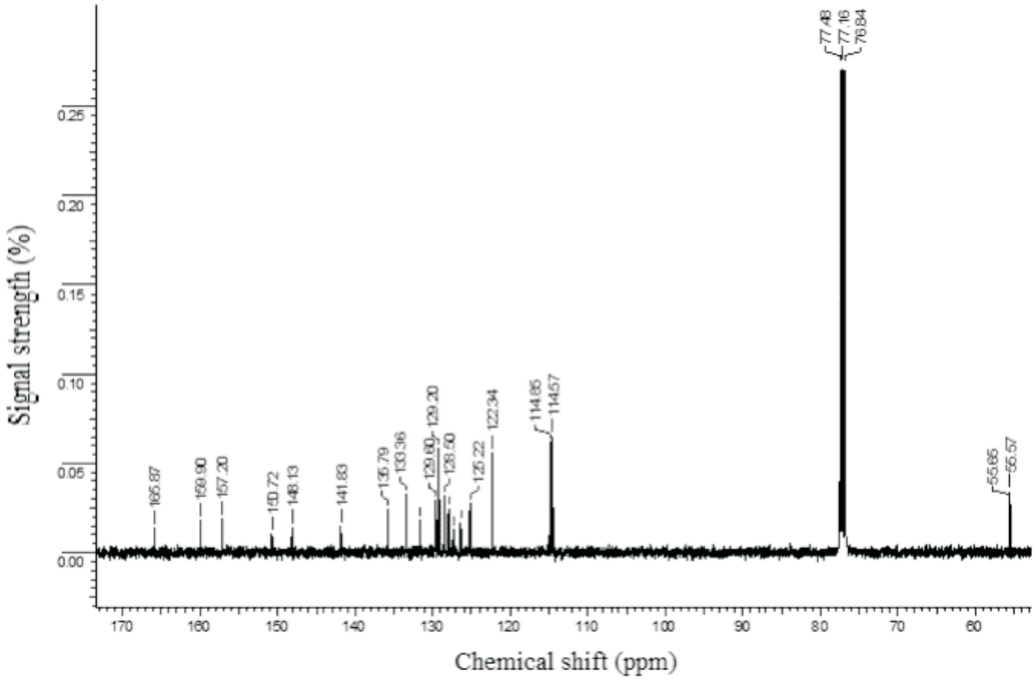

(b)

Figure 7 (**a**) ^{13}C NMR chemical shift and (**b**) calculated ^{13}C NMR for MNTZ.

doublet of doublets at 6.71 ppm (calculated at 6.95 ppm) while H7 and H9 appear as multiplet in 7.43–7.67 ppm range, corresponding calculated values at 7.72 and 7.55 ppm, respectively.

The experimental and calculated ^{13}C NMR spectra of MNTZ in chloroform are found at the range 55–165 ppm and 52–159 ppm and are shown in Fig. 7a and Fig. 7b, respectively. Among the carbon atoms, C11 gives the highest NMR chemical shift which is about 165.87 ppm, the corresponding estimated value is 159.32 ppm due to the effect of carbonyl moiety. The chemical shifts for C16 (observed at 159.9 and estimated at 153.4 ppm) and C22 (observed at 157.2 and estimated at 151.1 ppm) are found to be higher than the other phenyl carbons due to the electronegativity of the oxygen atoms. Also, the experimental signals of C1 and C12 appear in the higher frequency region at 148.13 and 150.72 ppm, respectively, the corresponding calculated values are 144.74 and 146.01 ppm, respectively, due to the nitrogen atoms. The other phenyl carbons NMR peaks are observed in the region of 114–135 ppm whereas the calculated ones range between 105 and 136 ppm. The signals for the allylidene fragment carbons (C7, C8, and C9) are observed at 141.8, 125.2 and 129.6 ppm while the calculated values are 136.9, 123.6 and 127.0 ppm, respectively. The carbon atoms C25 and C26 of the methoxy group give peaks at 55.65 and 55.57 ppm which is in agreement with the calculated values of 53.01 and 52.85 ppm,

respectively. All these results show that the B3LYP functional with the GIAO method and 6-31G(d,p) basis set, using chloroform as solvent predicted well the ^{1}H and ^{13}C NMR spectra.

3.4. Natural Bond Orbital (NBO) Analysis

NBO analysis has been performed using NBO 3.1[37] implemented in the Gaussian 09 program at DFT/B3LYP/6-31G(d,p) level to elucidate the conjugation, charge transfer and delocalization of electron density within the molecule.[38] In NBO analysis large E(2) value shows intensive interaction between electron-donors and electron acceptors and therefore indicating a greater extent of conjugation in the system.[39] The intramolecular hyper-conjugative interactions are formed by the orbital overlap between bonding π(C–C) and antibonding π^*(C–C) orbitals. These interactions have greater energy contributions from 10.16 to 24.25 Kcal mol^{-1} as depicted in Table 1. The

Table 1 Second-order perturbation theory analysis of the Fock matrix in the NBO basis for MNTZ.

Type	Donor (i)	Occupancy	Acceptor (j)	Occupancy	E(2)/kcal mol^{-1}	E(j)–E(i)/a.u.	F(i.j)/a.u.
π–π^*	C1–C2	1.651	C3–C4	0.335	17.21	0.29	0.064
			C5–C6	0.362	20.40	0.29	0.069
			O2–N1	0.625	26.28	0.15	0.061
π–π^*	C3–C4	1.618	C1–C2	0.374	24.25	0.27	0.073
			C5–C6	0.362	20.28	0.28	0.067
π–π^*	C5–C6	1.606	C1–C2	0.374	19.18	0.27	0.065
			C3–C4	0.335	21.69	0.28	0.070
			C7–C8	0.141	10.16	0.30	0.053
π–π^*	C7–C8	1.819	C5–C6	0.362	10.88	0.29	0.052
			C9–C10	0.232	19.22	0.30	0.068
π–π^*	C9–C10	1.827	C7–C8	0.141	13.41	0.32	0.059
			C11–O3	0.301	19.78	0.29	0.070
π–π^*	C13–C18	1.688	C14–C15	0.311	21.93	0.29	0.071
			C16–C17	0.394	16.26	0.28	0.062
π–π^*	C14–C15	1.701	C13–C18	0.371	17.54	0.28	0.064
			C16–C17	0.394	22.15	0.28	0.071
π–π^*	C16–C17	1.656	C13–C18	0.371	23.48	0.29	0.074
			C14–C15	0.311	16.22	0.30	0.062
π–π^*	C19–C20	1.672	C21–C22	0.394	17.91	0.28	0.064
			C23–C24	0.309	19.35	0.29	0.067
π–π^*	C21–C22	1.669	C19–C20	0.387	20.83	0.29	0.070
			C23–C24	0.309	17.00	0.30	0.064
π–π^*	C23–C24	1.719	C19–C20	0.387	17.91	0.28	0.065
			C21–C22	0.394	20.49	0.28	0.069
π–π^*	O2–N1	1.983	LP(3)O1	1.442	11.79	0.18	0.078
n–π^*	LP(2) S1	1.771	C9–C10	0.232	21.14	0.28	0.069
			C12–N3	0.296	22.15	0.27	0.071
n–s*	LP(2) O1	1.896	C1–N1	0.101	12.86	0.56	0.076
			O2–N1	0.065	19.04	0.69	0.104
n–π^*	LP(3) O1	1.442	O2–N1	0.625	156.71	0.15	0.139
n–s*	LP(2) O2	1.896	C1–N1	0.101	12.00	0.57	0.074
n–s*	LP(2) O2	1.896	O1–N1	0.061	19.52	0.70	0.106
n–s*	LP(2) O3	1.843	C10–C11	0.077	20.89	0.67	0.108
			C11–N2	0.095	29.61	0.66	0.127
n–π^*	LP(2) O4	1.837	C16–C17	0.394	31.39	0.34	0.098
n–π^*	LP(2) O5	1.842	C21–C22	0.394	30.36	0.34	0.096
n–π^*	LP(1) N2	1.622	C11–O3	0.301	53.95	0.27	0.111
			C12–N3	0.296	44.47	0.28	0.102
n–s*	LP(1) N3	1.817	C12–S1	0.107	25.65	0.46	0.099
π^*–π^*	C5–C6	0.362	C7–C8	0.141	50.24	0.02	0.062
π^*–π^*	C9–C10	0.232	C7–C8	0.141	84.32	0.01	0.068
π^*–π^*	C11–O3	0.301	C9–C10	0.232	124.94	0.01	0.073
π^*–π^*	C12–N3	0.296	C19–C20	0.387	36.22	0.02	0.043
π^*–π^*	C16–C17	0.394	C14–C15	0.311	243.66	0.01	0.081
π^*–π^*	C21–C22	0.394	C23–C24	0.309	261.82	0.01	0.082
π^*–π^*	O2–N1	0.625	C1–C2	0.374	15.29	0.13	0.057

E(2) stabilization energy (energy of hyper conjugative interaction).
E(j)–E(i) energy difference between donor (i) and acceptor (j) NBO orbitals.
F(i.j) Fock matrix element between i and j NBO orbitals.
LP Lewis type lone pair orbital.

intramolecular interactions are also due to the overlap between lone pair of oxygen, nitrogen and sulfur atoms and antibonding of (C–C), (C–N), (O–N) and (C–O) orbitals. For example, the strong intramolecular hyperconjugative interaction n(O1) → π^*(O2–N1) leads to stabilization energy of 156.71 Kcal mol^{-1}. Furthermore, the electron lone pair in the nitrogen of thiazolidinones ring LP(1) N2 transfer its electron to antibonding orbital π^*(C11–O3) and π^*(C12–N3) with stabilization energy of 53.95 and 44.47 Kcal mol^{-1}, respectively. Besides, the most important interactions are mainly from π^*(C11–O3), π^*(C21–C22) and π^*(C16–C17) orbitals as donor to the antibonding π^*(C9–C10), π^*(C23–C24) and π^*(C14–C15) orbitals as acceptor with a strong stabilization energy of 124.94, 261.82 and 243.66 Kcal mol^{-1}, respectively. All these intra-molecular hyper-conjugative interactions result in intra-molecular charge transfer (ICT) causing stabilization of the system.[40]

3.5. Chemical Stability and Electronic Transitions

3.5.1. *Frontier Molecular Orbitals (FMOs)*

The Frontier molecular orbitals (HOMO and LUMO) play a crucial role in the chemical stability and optical properties of the molecule, as well as in quantum chemistry and UV–Vis spectrum.[41,42] The HOMO, LUMO and band gap energies calculated at B3LYP and PBE functionals with 6-31G(d,p) basis set are listed in Table 2. The distributions of the HOMO and LUMO orbitals computed at the B3LYP/6-31G(d,p) method are shown in Fig. 8. It is interesting to see that both orbitals are substantially distributed over the conjugation plane. As can be seen from Fig. 8, the HOMO orbital is delocalized over the two methoxy-phenyl and imino-thiazolidinone rings whereas the LUMO orbital is localized on the nitro-phenyl and allylidene fragment. This intra-molecular charge transfer from the electron donating group through the π-conjugation system to the electron accepting group promotes the molecular stability.

Table 2 Calculated energies values of MNTZ calculated by B3LYP/6-31g(d,p) and PBE/6-31g(d,p) levels.

Parameters	6-31G (d,p)	
	B3LYP	PBE
E/ua	–1941.88	–1939.89
E_{HOMO}/ev	–5.4295	–4.6806
E_{LUMO}/ev	–2.7130	–3.3323
$\Delta E_{HOMO-LUMO\ gap}$/ev	2.7165	1.3483
Dipole moment (Debye)	5.9486	6.2585

3.5.2. *Global Chemical Reactivity Descriptors (GCRD)*

Nowadays, the chemical hardness and softness properties of a molecule are used to describe the reactivity and molecular stability. This relationship can be achieved by the determination of global chemical reactivity descriptor (GCRD) parameters. Using computational methods, GCRD parameters were calculated at the B3LYP and PBE level of theory with 6-31G(d,p) basis set by using the following equations:

$$\eta = \tfrac{1}{2}(1 - A)$$

$$\mu = -\left(\frac{I + A}{2}\right)$$

$$S = \frac{1}{2\eta}$$

$$\chi = -\left(\frac{I + A}{2}\right)$$

$$\omega = \frac{\mu^2}{2\eta}$$

where I = $-E_{HOMO}$ and A = $-E_{LUMO}$ are the ionization potential and electron affinity, respectively. The computed values of GCRD parameters are summarized in Table 3. The chemical hardness (η) values for the title compound are 1.358 and 0.674 eV as obtained by B3LYP and PBE functionals, respectively, where the small ETA-ETA-ETA values indicate that the charge transfer occurs in the molecule.

From the results, the calculated ionization potential, electron affinity and electronegativity using B3LYP (PBE) functional are 5.429 (4.680), 2.713 (3.332) and 4.071 (4.006) eV, respectively. According to these quantum chemical parameters, the MNTZ is a chemically hard system and can be described as a less reactive compound. Furthermore, the high values of the electrophilicity index (6.102 eV by B3LYP and 11.905 eV by PBE) compared to the

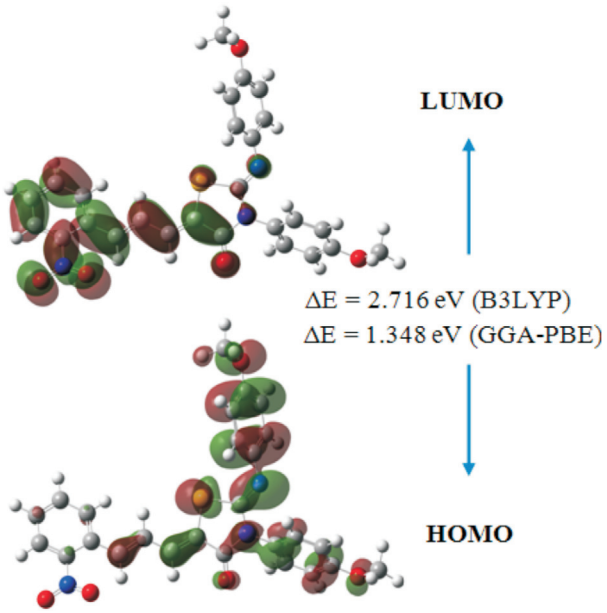

Figure 8 HOMO and LUMO plot of MNTZ.

Table 3 Calculated energy values of MNTZ by B3LYP and PBE methods.

Parameters	Calculated energies/eV	
	B3LYP/6-31G(d,p)	PBE/6-31G(d,p)
Ionization potential (I)	5.429	4.680
Electron affinity (A)	2.713	3.332
Electronegativity (χ)	4.071	4.006
Chemical potential (μ)	–4.071	–4.006
Chemical hardness (η)	1.358	0.674
Chemical softness (s)	0.368	0.741
Electrophilicity index (ω)	6.102	11.905

low values of chemical potential (–4.071 eV by B3LYP and –4.006 eV by PBE) for the MNTZ prove its electrophilic character. The chemical potential (μ) negative values indicate also the molecular stability of MNTZ. Softness is one of the material properties that measures the extent of chemical reactivity. The MNTZ has low chemical softness values 0.368 eV (B3LYP) and 0.741 eV (PBE), which measure the degree of chemical reactivity.

3.5.3. *Absorption Spectra*

For a molecule to have an important molecular charge transfer, it must show good absorption and emission properties. TD-DFT is often used to compute the excited-state properties of molecules.[43,44] From the optimized structure obtained by B3LYP/6-31G(d,p) level of the title compound, the electronic transitions were investigated by using the TD-DFT. The obtained results (vertical excitation energies, oscillator strength (f), transition wavelength and contributions) are collected in Table 4.

The experimental and calculated UV-Visible absorption spectra are shown in Fig. 9. As can be seen from Fig. 9a, there are two peaks observed at 348 and 406 nm, which are in the ultraviolet region. The corresponding calculated absorption peaks have been found at λ = 342.90 nm, f = 0.2430 and λ = 405.85 nm, f = 0.378. The other important transition in the calculated UV-Visible spectrum (Fig. 9b) is found at λ = 522.01 nm, f = 0.1519 which is in the visible region and corresponds to the HOMO → LUMO (98 %) transition. The transition simulated at 405.85 nm is comprised of HOMO → LUMO + 1 (49 %) and HOMO-2 → LUMO (42 %) transitions. The electronic excitation contributions from HOMO-8 and HOMO-2 to LUMO and LUMO+1 contribute to the transition which occurs at 342.9 nm. The absorption wavelength at 522 nm attributed to the intramolecular charge transfer (ICT) excitation between donor and acceptor moieties. According to the TD-DFT calculations, the experimental bands at 411 and 356 nm corresponding to π–π* and n–π* transitions. There is a good agreement between experimental and theoretical results.

3.6. Molecular Properties

3.6.1. *Mulliken and NBO Atomic Charges*

Atomic charge calculations play an important role in the application of quantum chemical calculations to the molecular system. The calculated Mulliken[45] and NBO charge values using B3LYP and PBE functionals with 6-31G(d,p) basis set are listed in Table 5. As can be seen, the results of Table 5 reveal the effect of the functional in the value of atomic charge distribution but the same behavior is observed. In fact, for hydrogen atoms, the difference is about 0.01 e and for the non-hydrogen atoms, it does not exceed 0.04 e. The Mulliken atomic charge analysis of MNTZ shows that nitrogen atoms (N2 and N3) have maximum negative charge values which impose positive charges to all carbon atoms bonded to these high electronegative atoms, while the nitrogen atom (N1) posses positive charge which was imposed by oxygen atoms (O1 and O2). The NBO atomic charge analysis of MNTZ shows that oxygen atoms (O3, O4 and O5) have maximum negative charge values. On the other hand, the maximum positive charge value is obtained for the C11 atom (for both Mulliken and NBO charges) due to the negative charge of oxygen (O3). Furthermore, O4 and O5 atoms have high negative charges which impose positive charges to C16 and C22, respectively. Moreover, all the hydrogen atoms have net positive charges thereby all carbon atoms connected to these electropositive atoms exhibit negative charges.

Table 4 Absorption spectrum data obtained by TD-DFT method at B3LYP/6-31g(d,p) level (Contribution ≥ 10 %)

Electronic transitions	λ_{abs}/nm	E_{ex}/eV	F	MO Contributions
S0→S1	522.01	2.3751	0.1519	HOMO → LUMO (98 %)
S0→S2	427.31	2.9015	0.0630	HOMO–1 → LUMO (64 %) HOMO → LUMO+1 (25 %)
S0→S3	419.50	2.9555	0.0159	HOMO–2 → LUMO (44 %) HOMO–1 → LUMO (28 %) HOMO → LUMO+1 (24 %)
S0→S4	405.85	3.0549	0.3786	HOMO → LUMO+1 (49 %) HOMO–2 → LUMO (42 %)
S0→S5	348.64	3.5562	0.1584	HOMO–1 → LUMO+1 (89 %)
S0→S6	342.90	3.6158	0.2430	HOMO–2 → LUMO+1 (62 %) HOMO–8 → LUMO (14 %)
S0→S7	335.18	3.6991	0.1280	HOMO–2 → LUMO+1 (26 %) HOMO–8 → LUMO (22 %) HOMO–10 → LUMO (18 %)
S0→S8	331.19	3.7436	0.0226	HOMO–3 →→ LUMO (62 %) HOMO–6 → LUMO (10 %)
S0→S9	322.74	3.8416	0.0104	HOMO–4 → LUMO (80 %) HOMO–3 → LUMO (16 %)
S0→S10	315.86	3.9253	0.0110	HOMO–6 → LUMO (30 %) HOMO–5 → LUMO (28 %) HOMO–3 → LUMO (16 %)

3.6.2. *Molecular Electrostatic Potential*

The main purpose of the molecular electrostatic potential study is the localization of electrophilic and nucleophilic sites of a molecule.[46] In the MEP map, the red colour indicates the maximum negative region promoting the site for an electrophilic attack while the blue colour indicates the maximum positive region making the site favorable for nucleophilic attack. Molecular electrostatic potential of MNTZ using B3LYP/6-31G (d,p) optimized geometry is computed and its surface map is shown in Fig. 10. This MEP map shows that there are three possible sites for electrophilic attack localized on the O1, O2, and O3 atoms, while the sites for the nucleophilic attack are located over the hydrogen atoms. The region very near to the sulfur atom is positive due to the fact that the S atom is surrounded by the electropositive atoms. These results show that the most reactive site of the MNTZ molecule is the site containing the oxygen atoms. These sites give information concerning the region from where the compound can have intermolecular interactions.

3.7. Thermodynamic Properties

The values of some thermodynamic parameters (such as zero-point vibrational energy (ZPVE), rotational constants, rotational temperatures, thermal energy, molecular capacity at constant volume, entropy, zero point correction, thermal correction

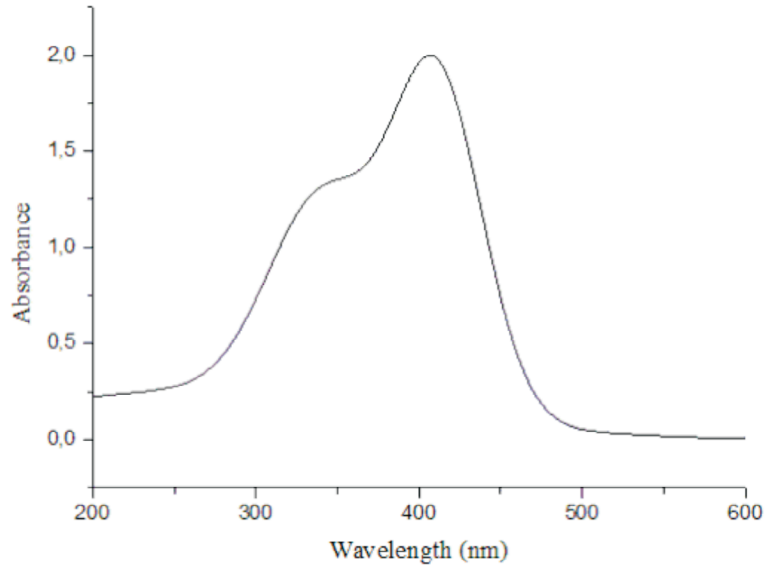

(a)

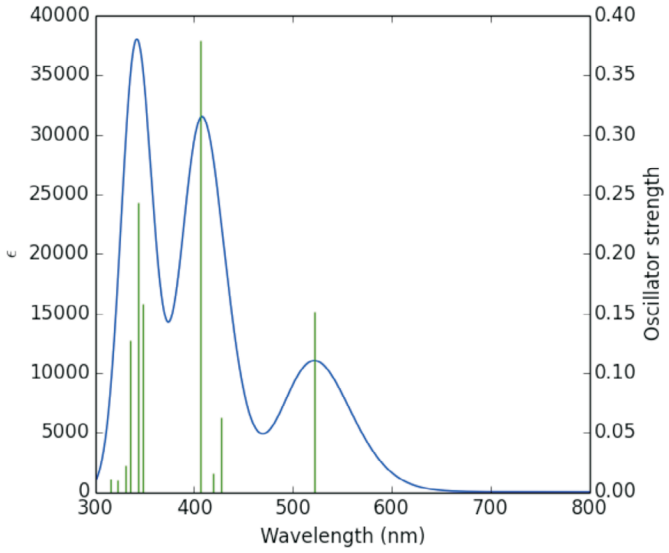

(b)

Figure 9 The (**a**) experimental UV-Vis and (**b**) simulated UV-Vis spectra of MNTZ.

to energy, thermal correction to enthalpy and thermal correction to Gibbs Free Energy) of MNTZ at 298.15 K in ground state are obtained from the theoretical harmonic frequencies and reported in Table S7. The variation in zero-point vibrational energies (ZPVEs) seems to be considerable. The ZPVE obtained from B3LYP functional is higher compared to the value obtained from the PBE functional. Whereas, no change was observed for rotational constant and rotational temperature using both functionals. The total energy of the MNTZ molecule is the sum of electronic, translational, rotational and vibrational energies, even for entropy and capacity at constant volume. The thermodynamic functions such as entropy (S), heat capacity at constant pressure (Cp) and enthalpy content ($\Delta H = H(T) - H(0)$) for various ranges of temperatures from 100 to 1000 K are determined using perl script THERMO.PL[47] and reported in Table S8 and Fig. 11. It is obvious to see that the change of the functional does not affect the thermodynamic properties at different temperatures. Furthermore, all the calculated thermody-

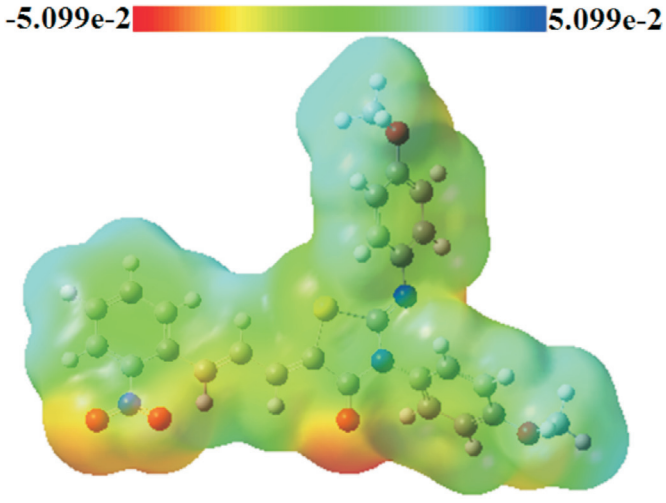

Figure 10 Molecular electrostatic potential surface for MNTZ.

Table 5 Mulliken and NBO atomic charges of MNTZ using B3LYP/6-31g(d,p) and PBE/6-31g(d,p) levels.

Atoms	Mulliken charges		NBO charges		Atoms	Mulliken charges		NBO charges	
	B3LYP	PBE	B3LYP	PBE		B3LYP	PBE	B3LYP	PBE
S1	0.213	0.241	0.316	0.334	C20	–0.105	–0.117	–0.251	–0.263
O1	–0.386	–0.358	–0.382	–0.358	C21	–0.145	–0.156	–0.316	–0.325
O2	–0.391	–0.363	–0.380	–0.356	C22	0.352	0.329	0.312	0.294
O3	–0.488	–0.454	–0.572	–0.535	C23	–0.122	–0.134	–0.267	–0.277
O4	–0.517	–0.478	–0.517	–0.480	C24	–0.093	–0.106	–0.225	–0.234
O5	–0.519	–0.479	–0.520	–0.482	C25	–0.081	–0.149	–0.329	–0.375
N1	0.359	0.323	0.511	0.472	C26	–0.078	–0.147	–0.328	–0.374
N2	–0.605	–0.568	–0.469	–0.432	H2	0.141	0.147	0.276	0.284
N3	–0.524	–0.499	–0.483	–0.452	H3	0.108	0.117	0.252	0.260
C1	0.191	0.188	0.079	0.077	H4	0.106	0.116	0.251	0.259
C2	–0.081	–0.097	–0.211	–0.226	H5	0.107	0.114	0.205	0.257
C3	–0.097	–0.110	–0.231	–0.239	H7	0.127	0.137	0.262	0.272
C4	–0.069	–0.083	–0.207	–0.222	H8	0.101	0.111	0.232	0.240
C5	–0.133	–0.140	–0.211	–0.217	H9	0.137	0.144	0.250	0.278
C6	0.115	0.110	–0.052	–0.063	H14	0.106	0.120	0.257	0.269
C7	–0.088	–0.105	–0.183	–0.195	H15	0.101	0.112	0.254	0.263
C8	–0.088	–0.101	–0.232	–0.239	H17	0.091	0.101	0.245	0.255
C9	–0.065	–0.075	–0.203	–0.222	H18	0.101	0.114	0.253	0.265
C10	–0.227	–0.246	–0.286	–0.288	H20	0.100	0.115	0.247	0.257
C11	0.624	0.585	0.677	0.621	H21	0.087	0.098	0.243	0.253
C12	0.325	0.283	0.329	0.290	H23	0.097	0.109	0.252	0.261
C13	0.248	0.233	0.115	0.111	H24	0.097	0.109	0.252	0.261
C14	–0.058	–0.071	–0.207	–0.224	H25a	0.114	0.131	0.207	0.219
C15	–0.134	–0.147	–0.271	–0.278	H25b	0.127	0.143	0.233	0.245
C16	0.363	0.339	0.327	0.305	H25c	0.115	0.131	0.207	0.219
C17	–0.151	–0.161	–0.320	–0.327	H26a	0.111	0.128	0.205	0.217
C18	–0.062	–0.075	–0.199	–0.216	H26b	0.125	0.141	0.232	0.244
C19	0.209	0.203	0.104	0.096	H26c	0.112	0.129	0.205	0.217

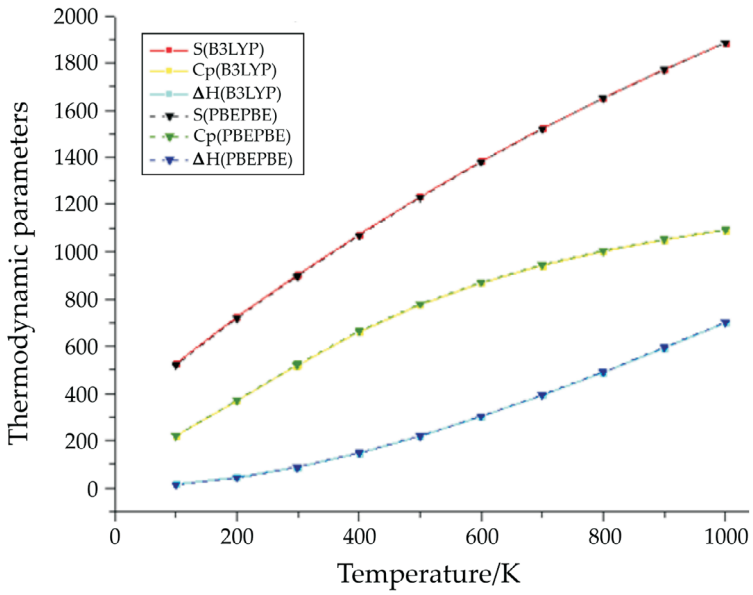

Figure 11 The thermodynamic properties of MNTZ calculated with B3LYP and PBE functionals.

namic parameters (S, C_p, and ΔH) increase with the increase of temperature, due to the enhancement of molecular vibration.

4. Conclusions

In the present work, the optimized molecular geometry of thiazolidinones derivative has been investigated and compared with its X-ray structure. The structure was optimized using DFT/B3LYP and PBE methods with 6-31g(d,p) basis set. Bond lengths, as described earlier, are similar to literature values. Bond angles indicate that the π electrons in the studied molecule are delocalized. Except for some values, the obtained results indicate the good agreement between calculated values and experimental parameters. Detailed experimental spectroscopic results were presented. The vibrational wavenumbers of the title compound have been calculated by B3LYP and PBE functionals with 6-31G(d,p) basis set and assigned on the basis of PED. The experimental and theoretical frequencies were compared taking into account the scaling factors 0.961 and 0.986 for B3LYP and

PBE, respectively. Gauge independent atomic orbital (GIAO) was used to calculate ^{1}H and ^{13}C NMR spectra. The results showed that, in general, the calculated and experimental chemical shift values were consistent. Hyperconjugative interaction and charge transfer within the molecule were explained by NBO analysis which indicates that the most intra-molecular interactions are due to the overlap between lone pair of O, N and S atoms and antibonding of (C–C), (C–N), (O–N) and (C–O) orbitals. The computed HOMO-LUMO energy gap and the global chemical reactivity descriptors quantum parameters explain the significant charge transfer interactions taking place within the molecule and promotes the molecular stability. Mulliken charges and MEP analysis allow the identification of electrophilic and nucleophilic sites in the molecule and give information about intermolecular interaction regions. Furthermore, the thermodynamic properties of the compound have been calculated and their values at different temperatures are also obtained.

Supplementary Material

Supplementary information is provided in the online supplement.

§ORCID iD

R. Rahmani: orcid.org/0000-0002-0335-8783

References

1 M.A. Badawy, N.H. Metwally and D.S. Okpy, Synthesis of some new 5-substituted-3-phenyl-4-thioxo-2-thiazolidinones and their fused thiopyrano[2,3-d]thiazole derivatives, *J. Sulfur Chem.*, 2015, **36**(5), 511–525.

2 S.K. Patil, B.P. Langi and H.P. Deokar, Synthesis and characterization of some novel bioactive thiazolidinone derivatives of 3-substituted coumarin, *Ind. Am. J. Pharm. Res.*, 2015, **5**(1), 578–583.

3 R. Gupta, Recent advances in chemistry of condensed 4-thiazolidinones. *J. Heterocyclic Chem.*, 2016, **53**, 1687–1696.

4 E. Hamade, A. Habib, A. Hachem, A.H. Hussein, M. Abbas, T. Hirz, M. Al-Masri and W.H. Faour, Biological and anti-inflammatory evaluation of two thiazole compounds in RAW cell line: potential cyclooxygenase-2 specific inhibitors, *Med. Chem.*, 2012, **8**(3), 401–408.

5 A. Nowaczyk, M. Kowiel, A. Gzella, Ł. Fijałkowski, V. Horishny and R. Lesyk, Conformational space and vibrational spectra of 2-[(2,4-dimethoxyphenyl)amino]-1,3-thiazolidin-4-one, *J. Mol. Model.*, 2014, **20**, 2366–2375.

6 A. Kunzler, P.D. Neuenfeldt, A.M. das Neves, C.M.P. Pereira, G.H. Marques, P.S. Nascente, M.H.V. Fernandes, S.O. Hübner and W. Cunico, Synthesis, antifungal and cytotoxic activities of 2-aryl-3-((piperidin-1-yl)ethyl)thiazolidinones, *Eur. J. Med. Chem.*, 2013, **64**, 74–80.

7 M. Asif, Pharmacologically potentials of different substituted coumarin derivatives, *Chem. Int.*, 2015, **1**(1), 1–11.

8 D. Gautam and R.P. Chaudhary, Synthesis, structure and antimicrobial evaluation of new 3,3a,4,5-tetrahydro-2H-benzo[g]indazol-2-yl-thiazol-4(5H)-ones, *Spectrochim. Acta A.*, 2015, **135**, 219–226.

9 V. Smokal, B. Derkowska, R. Czaplicki, O. Krupka, A. Kolendo and B. Sahraoui, Nonlinear optical properties of thiazolidinone derivatives, *Opt. Mater.*, 2009, **31**(3), 554–557.

10 A.S. Yapi, L. Toumi, Y. Lare, G.M. Soto, L. Cattin, K. Toubal, A. Djafri, M. Morsli, A. Khelil, M.A. Del Valle and J.-C. Bernède, On the influence of the exciton-blocking layer on the organic multilayer cells properties, *Eur. Phys. J. Appl. Phys.*, 2010, **50**(3), 30403:1–30403:8.

11 R. Rahmani, A. Djafri, J.-C. Daran, A. Djafri, A. Chouaih and F. Hamzaoui, Crystal structure of (2Z,5Z)-3-(4-methoxyphenyl)-2-[(4-methoxyphenyl) imino]-5-[(E)-3-(2-nitrophenyl)allylidene]-1,3-thiazolidin-4-one, *Acta Cryst. E.*, 2016, **72**, 155–157.

12 R. Rahmani, A. Djafri, A. Chouaih, A. Djafri, F. Hamzaoui, R. Rizzi and A. Altomare, Synthesis, molecular and solid-state structure of 5-(5-nitrofuran-2-ylmethylen), 3-N-(2-methoxy phenyl), 2-N′-(2-methoxyphenyl) imino thiazolidin-4-one: X-ray powder diffraction and DFT studies, *J. Mol. Struct.*, 2017, **1143**, 259–264.

13 N. Khelloul, K. Toubal, N. Benhalima, R. Rahmani, A. Chouaih, A. Djafri and F. Hamzaoui, Crystal structure, Hirshfeld surface analysis and computational studies of thiazolidin-4-one derivative: (Z)-5-(4-Chlorobenzylidene)-3-(2-ethoxyphenyl)-2-thioxothiazolidin-4-one, *Acta Chim. Slov.*, 2016, **63**, 619–626.

14 K. Toubal, A. Djafri, A. Chouaih and A. Talbi, Synthesis and structural determination of novel 5-arylidene-3-N(2-alkyloxyaryl)-2-thioxo-thiazolidin-4-ones, *Molecules.*, 2012, **17**, 3501–3509.

15 N. Benhalima, K. Toubal, A. Chouaih, G. Chita, S. Maggi, A. Djafri and F. Hamzaoui, Synthesis and molecular structure investigation by DFT and X-ray diffraction of ARNO, *J. Chem. Crystallogr.*, 2011, **41**, 1729–1736.

16 M.J. Frisch, G.W. Trucks, H.B. Schlegel, G.E. Scuseria, M.A. Robb, J.R. Cheeseman, G. Scalmani, V. Barone, B. Mennucci, G.A. Petersson, H. Nakatsuji, M. Caricato, X. Li, H.P. Hratchian, A.F. Izmaylov, J. Bloino, G. Zheng, J.L. Sonnenberg, M. Hada, M. Ehara, K. Toyota, R. Fukuda, J. Hasegawa, M. Ishida, T. Nakajima, Y. Honda, O. Kitao, H. Nakai, T. Vreven, J.A. Montgomery, Jr, J.E. Peralta, F. Ogliaro, M. Bearpark, J.J. Heyd, E. Brothers, K.N. Kudin, V.N. Staroverov, R. Kobayashi, J. Normand, K. Raghavachari, A. Rendell, J.C. Burant, S.S. Iyengar, J. Tomasi, M. Cossi, N. Rega, J.M. Millam, M. Klene, J.E. Knox, J.B. Cross, V. Bakken, C. Adamo, J. Jaramillo, R. Gomperts, R.E. Stratmann, O. Yazyev, A. J. Austin, R. Cammi, C. Pomelli, J.W. Ochterski, R.L. Martin, K. Morokuma, V.G. Zakrzewski, G.A. Voth, P. Salvador, J.J. Dannenberg, S. Dapprich, A.D. Daniels, E.O. Farkas, J.B. Foresman, J.V. Ortiz, J. Cioslowski and D.J. Fox, Gaussian 09, Gaussian Inc, Wallingford, CT, 2009.

17 A. Frisch, A.B. Nielson and A.J. Holder, *GaussView User Manual*. Gaussian Inc, Pittsburgh, 2000.

18 A.D. Becke, Density-functional thermochemistry. III. The role of exact exchange, *J. Chem. Phys.*, 1993, **98**, 5648–5652.

19 C. Lee, W. Yang and R.G. Parr, Development of the Colle-Salvetti correlation-energy formula into a functional of the electron density, *Phys. Rev. B.*, 1988, **37**, 785–789.

20 J.P. Perdew, K. Burke and M. Ernzerhof, Generalized gradient approximation made simple [Phys. Rev. Lett. **77**, 3865 (1996)], *Phys. Rev. Lett.*, 1997, **78**, 1396–1396.

21 M.H. Jamroz, *Vibrational Energy Distribution Analysis VEDA 4*, Warsaw, 2004.

22 J.B. Foresman, M. Head-Gordon, J.A. Pople and M.J. Frisch, Toward a systematic molecular orbital theory for excited states, *J. Phys. Chem.*, 1992, **96(1)**, 135–149.

23 P. Pulay, G. Fogarasi, G. Pongor, J.E. Boggs and A. Vargha, Combination of theoretical ab initio and experimental information to obtain reliable harmonic force constants. Scaled quantum mechanical (QM) force fields for glyoxal, acrolein, butadiene, formaldehyde, and ethylene, *J. Am. Chem. Soc.*, 1983, **105**(24), 7037–7047.

24 NIST Computational Chemistry Comparison and Benchmark Database NIST Standard Reference Database Number 101 Release 16a, Editor: Russell D. Johnson III, 2013, http://cccbdb.nist.gov/

25 R.A. Nyquist, *Interpreting Infrared, Raman, and Nuclear Magnetic Resonance Spectra*, Volume 1, Academic Press, 2001.

26 G. Socrates, Infrared and Raman characteristic group frequencies tables and charts, 3rd edn., Wiley, 2001.

27 S. Renuga, M. Karthikesan and S. Muthu, FTIR and Raman spectra, electronic spectra and normal coordinate analysis of N,N-dimethyl-3-phenyl-3-pyridin-2-yl-propan-1-amine by DFT method, *Spectrochim. Acta A: Mol. Biomol. Spectrosc.*, 2014, **127**, 439–453.

28 M. Margoshes and V.A. Fassel, The infrared spectra of aromatic compounds: I. The out-of-plane C-H bending vibrations in the region 625–900 cm-^{1}, *Spectrochim. Acta*, 1955, **7**, 14–24.

29 B.H. Stuart, *Infrared Spectroscopy: Fundamentals and Applications*, Wiley, Chichester, 2004.

30 Shamsuzzaman, K.A.A. Abdul Baqi, A. Ali, M. Asif, A. Mashrai, H. Khanam, A. Sherwani, Z. Yaseen and M. Owais, Synthesis, characterization, biological evaluation and molecular docking of steroidal spirothiazolidinones, *J. Mol. Struct.*, 2015, **1085**, 104–114.

31 V. Balachandran, G. Santhi, V. Karpagam, B. Revathi and M. Karabacak, Spectroscopic investigation, natural bond orbital analysis, HOMO-LUMO and thermodynamic functions of 2-tert-butyl-5-methyl anisole using DFT (B3LYP) calculations, *Spectrochim. Acta A: Mol. Biomol. Spectrosc.*, 2015, **136**(Part B), 451–463.

32 P. Mehta, P. Dawedra, V. Goswami and H.S. Joshi, Synthesis and characterization of some thiazolidinone derivatives possessing benzimidazole nucleus, *Int. Lett. Chem. Phys. Astron.* 2014, **30**, 1–8.

33 M. Wolszleger, C.D. Stan, A. Pânzariu, A. Jităreanu and L. Profire, New thiazolidine-4-ones of ferulic acid with antioxidant potential, *Farmacia*., 2015, **63**(1), 150–154.

34 K. Wolinski, J.F. Hilton and P. Pulay, Efficient implementation of the gauge-independent atomic orbital method for NMR chemical shift calculations, *J. Am. Chem. Soc*., 1990, **112**(23), 8251–8260.

35 R. Rahmani, N. Boukabcha, A. Chouaih, F. Hamzaoui and S. Goumri-Said, On the molecular structure, vibrational spectra, HOMO-LUMO, molecular electrostatic potential, UV–Vis, first-order hyperpolarizability, and thermodynamic investigations of 3-(4-chlorophenyl)-1-(1yridine-3-yl) prop-2-en-1-one by quantum chemistry calculations, *J. Mol. Struct*., 2018, **1155**, 484–495.

36 J.A. Bohmann, F. Weinhold and T.C. Farrar, Natural chemical shielding analysis of nuclear magnetic resonance shielding tensors from gauge-including atomic orbital calculations, *J. Chem. Phys*., 1997, **107**, 1173–1184.

37 E.D. Glendening, A.E. Reed, J.E. Carpenter and F. Weinhold, NBO 3.1 Program Manual, Theoretical Chemistry Institute, University of Wisconsin, Madison, 1996.

38 F. Weinhold and C.R. Landis, *Discovering Chemistry with Natural Bond Orbitals*, John Wiley & Sons, New Jersey, 2012.

39 Y.B. Shankar Rao, M.V.S. Prasad, N. Udaya Sri and V. Veeraiah, Vibrational (FT-IR, FT-Raman) and UV–Visible spectroscopic studies, HOMO–LUMO, NBO, NLO and MEP analysis of benzyl (imino (1H-pyrazol-1-yl) methyl) carbamate using DFT calculaions, *J. Mol. Struct*., 2016, **1108**, 567–582.

40 N. Issaoui, H. Ghalla, F. Bardak, M. Karabacak, N. Aouled Dlala, H.T. Flakus and B. Oujia, Combined experimental and theoretical studies on the molecular structures, spectroscopy, and inhibitor activity of 3-(2-thienyl)acrylic acid through AIM, NBO, FT-IR, FT-Raman, UV and HOMO-LUMO analyses, and molecular docking, *J. Mol. Struct*., 2017, **1130**, 659–668.

41 S. Saravanan, V. Balachandran and K. Viswanathan, Spectroscopic investigation of 4-nitro-3-(trifluoromethyl)aniline, NBO analysis with 4-nitro-3-(trichloromethyl)aniline and 4-nitro-3-(tribromomethyl)aniline, *Spectrochim. Acta A: Mol. Biomol. Spectrosc*., 2014, **121**, 685–697.

42 I. Fleming, *Frontier Orbitals*, *Organic Chemical Reactions*, Wiley, London, 1976.

43 F. Furche and D. Rappoport, in Density functional methods for excited states' equilibrium structure and electronic spectra, in *Computational Photochemistry Theoretical and Computational Chemistry,* vol. 16 , (M. Olivucci, ed.), Elsevier, Amsterdam, 2005.

44 M.A.L. Marques, N.T. Maitra, F.M.S. Nogueira, E.K.U. Gross and A. Rubio, *Fundamentals of Time-dependent Density Functional Theory*, Springer-Verlag, Berlin Heidelberg, 2012.

45 R.S. Mulliken, Electronic population analysis on LCAOMO molecular wave functions. I, *J. Chem. Phys*., 1955, **23**, 1833–1840.

46 E. Scrocco and J. Tomasi, Electronic molecular structure, reactivity and intermolecular forces: An euristic interpretation by means of electrostatic molecular potentials, *Adv. Quantum Chem*., 1978, **11**, 115–193.

47 K.K. Irikura, *THERMO.PL*, National Institute of Standards and Technology, Gaithersburg, MD, 2002.

Supplementary material to:

R. Rahmani, Ah. Djafri, A. Chouaih, Ay. Djafri, F. Hamzaoui and A.M. Krallafa,

Molecular Structure, FT-IR, NMR ($^{13}C/^{1}H$), UV–Vis Spectroscopy and DFT Calculations on (2Z, 5Z)-3-N(4-Methoxy phenyl)-2-N′(4-methoxy phenyl imino)-5-((E)-3-(2-nitrophenyl)allylidene) thiazolidin-4-one,

S. Afr. J. Chem., 2019, **72**, 176–188.

Supplementary Information for

Molecular structure, FT-IR, NMR ($^{13}C/^{1}H$), UV–Vis spectroscopy and DFT calculations on (2Z, 5Z)-3-N(4-methoxy phenyl)-2-N'(4- methoxy phenyl imino)-5-((E)-3-(2-nitrophenyl)allylidene) thiazolidin-4-one

Rachida Rahmani[a,b], Ahmed Djafri[a,c], Abdelkader Chouaih[a], Ayada Djafri[d], Fodil Hamzaoui[a,e], Abdelghani M. Krallafa[f]

[a] Laboratory of Technology and Solid Properties (LTPS), Abdelhamid Ibn Badis University - Mostaganem, 27000 Mostaganem, Algeria
[b] Département de Génie des Procédés, Centre Universitaire Ahmed Zabana - Relizane, 48000 Relizane, Algérie
[c] Centre de Recherche Scientifique et Technique en Analyses Physico-chimiques (CRAPC), BP 384-Bou-Ismail-RP 42004, Tipaza-Algeria
[d] Laboratoire de Synthèse Organique Appliquée (LSOA), Département de Chimie, Faculté des Sciences, Université d'Oran 1 - Ahmed Ben Bella, 31000 Oran, Algérie
[e] LPFM Académie de Montpellier, France
[f] LCPM, Dpt of Chemistry, Faculty of Sciences, University of Oran 1, Ahmed Benbella, 31000, Algeria

Contents

Table S1: Atomic coordinates (xyz) of the optimized structure for MNTZ

Atoms	B3LYP			PBEPBE		
	x	*y*	*z*	*x*	*y*	*z*
S1	0.016787	0.671831	-0.088855	0.017602	0.672093	-0.098385
O1	-8.081380	-2.451031	0.874117	-8.160143	-2.403057	0.896011
O2	-5.959632	-2.525009	1.351256	-6.006085	-2.552478	1.300060
O3	0.461762	-3.172567	-0.227766	0.433301	-3.188622	-0.227557
O4	6.598275	-4.144933	-0.222611	6.575618	-4.222344	-0.189248
O5	2.920892	6.427342	-0.048464	3.033968	6.430556	-0.028586
N1	-6.941099	-1.988391	0.834102	-6.997036	-1.973577	0.820507
N2	1.797914	-1.280775	-0.124967	1.796443	-1.290473	-0.127952
N3	2.780203	0.847304	-0.144174	2.797654	0.840831	-0.165733
C1	-6.754504	-0.700361	0.142266	-6.792217	-0.678029	0.135771
C2	-7.900736	0.084170	0.005610	-7.937599	0.117211	-0.010767
C3	-7.815669	1.339350	-0.583432	-7.840288	1.385255	-0.584252
C4	-6.579684	1.791681	-1.052668	-6.589107	1.842666	-1.030211
C5	-5.449465	0.992310	-0.933899	-5.459616	1.034298	-0.905015
C6	-5.485430	-0.277517	-0.319724	-5.506962	-0.252360	-0.306945
C7	-4.268455	-1.091579	-0.259234	-4.297839	-1.070065	-0.245067
C8	-3.011472	-0.587814	-0.219777	-3.023630	-0.570428	-0.220316
C9	-1.841109	-1.422295	-0.214573	-1.863654	-1.409146	-0.215626
C10	-0.556904	-0.996422	-0.169030	-0.561501	-0.989769	-0.173982
C11	0.573017	-1.961046	-0.175815	0.556084	-1.966963	-0.177987
C12	1.745738	0.116989	-0.112907	1.749189	0.108970	-0.121089
C13	3.045723	-1.993545	-0.128200	3.038096	-2.011892	-0.123830
C14	3.326007	-2.897684	-1.158434	3.258129	-3.020273	-1.079990
C15	4.520272	-3.603176	-1.155992	4.450448	-3.740318	-1.068411
C16	5.455161	-3.408327	-0.128457	5.442861	-3.459606	-0.107499
C17	5.175245	-2.501252	0.900902	5.222715	-2.448486	0.847036
C18	3.967444	-1.803224	0.897783	4.018413	-1.733822	0.837161
C19	2.739662	2.251547	-0.084886	2.775998	2.240457	-0.092951
C20	2.100631	2.955334	0.944194	2.042072	2.962168	0.872201
C21	2.139181	4.351887	0.994121	2.103414	4.362000	0.930401
C22	2.823257	5.065364	0.005693	2.904309	5.066918	0.014224
C23	3.482417	4.366543	-1.018386	3.660511	4.352706	-0.939783
C24	3.452883	2.981782	-1.053743	3.609070	2.963364	-0.980578
C25	7.579217	-3.998109	0.793001	7.602972	-3.976767	0.768590
C26	2.276558	7.185041	0.962324	2.284581	7.187878	0.917430
H2	-8.839532	-0.306255	0.376720	-8.887733	-0.283332	0.346519
H3	-8.704132	1.954214	-0.680615	-8.732069	2.008679	-0.687482
H4	-6.499724	2.763501	-1.530080	-6.498075	2.827664	-1.497076
H5	-4.511037	1.334615	-1.355638	-4.506373	1.379164	-1.313840
H7	-4.390734	-2.167851	-0.234772	-4.425674	-2.153907	-0.201952
H8	-2.861073	0.488732	-0.164975	-2.865765	0.514815	-0.171534
H9	-1.972740	-2.501667	-0.252557	-1.996574	-2.497448	-0.248959
H14	2.603351	-3.054941	-1.950406	2.488960	-3.245520	-1.820404
H15	4.753604	-4.312173	-1.942761	4.639180	-4.529791	-1.799888
H17	5.879820	-2.331889	1.705726	5.974678	-2.211521	1.601912
H18	3.750916	-1.099960	1.693481	3.847731	-0.947953	1.575265
H20	1.590413	2.410315	1.731813	1.444170	2.422877	1.612281
H21	1.640647	4.862777	1.809061	1.532588	4.886763	1.699249
H23	4.019153	4.935397	-1.770378	4.289549	4.916228	-1.633846
H24	3.973485	2.439065	-1.835862	4.201892	2.405047	-1.709800
H25a	7.961880	-2.970724	0.840743	7.991935	-2.944073	0.695814
H25b	8.393585	-4.671940	0.523731	8.409078	-4.684670	0.531694
H25c	7.187190	-4.281488	1.777939	7.250979	-4.158012	1.801139
H26a	1.192225	7.013841	0.968796	1.196627	7.023002	0.804046
H26b	2.472355	8.231918	0.725886	2.514645	8.241943	0.709139
H26c	2.679399	6.959958	1.958420	2.577238	6.950823	1.957617

Table S2: Optimized bond lengths computed at B3LYP and PBE functionals with 6-31g(d,p) basis set

Bond length (Å)	X-ray[11]	6-31G(d,p)		Bond length (Å)	X-ray[11]	6-31G(d,p)	
		B3LYP	PBE			B3LYP	PBE
S1–C10	1.753 (3)	1.766	1.761	N2–C11	1.384 (3)	1.402	1.414
S1–C12	1.777 (2)	1.816	1.821	N2–C12	1.388 (3)	1.399	1.400
O1–N1	1.225 (3)	1.231	1.242	N2–C13	1.440 (3)	1.437	1.436
O2–N1	1.232 (3)	1.232	1.244	N3–C12	1.267 (3)	1.267	1.279
O3–C11	1.206 (3)	1.218	1.229	N3–C19	1.426 (4)	1.406	1.402
O4–C16	1.365 (3)	1.363	1.368	C6–C7	1.465 (3)	1.465	1.461
O4–C25	1.431 (3)	1.420	1.426	C7–C8	1.341 (3)	1.355	1.369
O5–C22	1.374 (4)	1.366	1.370	C8–C9	1.438 (3)	1.437	1.431
O5–C26	1.385 (5)	1.418	1.425	C9–C10	1.336 (4)	1.354	1.369
N1–C1	1.448 (3)	1.474	1.480	C10–C11	1.491 (4)	1.486	1.484

Table S3: Optimized bond angles computed at B3LYP and PBE levels with 6-31g(d,p) basis set

Bond angles (°)	X-ray[11]	6-31G(d,p)		Bond angles (°)	X-ray[11]	6-31G(d,p)	
		B3LYP	PBE			B3LYP	PBE
S1–C10–C9	126.1 (2)	127.36	127.10	N2–C13–C14	120.5 (2)	119.74	119.56
S1–C10–C11	111.0 (2)	111.50	111.94	N2–C13–C18	119.0 (2)	120.36	120.49
S1–C12–N2	110.7 (2)	109.93	109.95	N3–C19–C20	121.4 (3)	123.08	123.66
S1–C12–N3	125.0 (2)	126.99	127.07	N3–C19–C24	120.3 (3)	118.33	117.92
O1–N1–O2	122.5 (2)	124.08	124.17	C1–C6–C7	123.4 (2)	124.42	124.49
O1–N1–C1	118.4 (2)	117.44	117.42	C5–C6–C7	120.9 (2)	119.78	119.83
O2–N1–C1	119.2 (2)	118.47	118.40	C6–C7–C8	123.9 (3)	124.41	124.53
O3–C11–C10	125.5 (2)	125.22	125.40	C7–C8–C9	122.5 (3)	122.66	122.72
O3–C11–N2	124.6 (2)	124.34	124.39	C8–C9–C10	124.8 (3)	126.15	126.27
O4–C16–C15	116.1 (2)	115.67	115.54	C9–C10–C11	122.9 (2)	121.13	120.96
O4–C16–C17	124.0 (2)	124.64	124.78	C10–S1–C12	91.4 (1)	91.15	91.16
O5–C22–C21	124.2 (3)	124.87	124.96	C11–N2–C12	116.9 (2)	116.91	116.67
O5–C22–C23	115.8 (3)	115.69	115.58	C11–N2–C13	120.9 (2)	121.19	121.22
N1–C1–C2	116.1 (2)	115.67	115.59	C12–N2–C13	122.1 (2)	121.87	122.09
N1–C1–C6	121.6 (2)	121.86	122.03	C12–N3–C19	116.1 (2)	123.45	123.83
N2–C11–C10	109.9 (2)	110.44	110.21	C16–O4–C25	116.7 (2)	118.30	117.41
N2–C12–N3	124.3 (2)	123.06	122.91	C22–O5–C26	118.8 (3)	118.15	117.28

Table S4: Optimized dihedral angles computed at B3LYP and PBE functionals with 6-31g(d,p) basis set

Dihedral angles (°)	X-ray[11]	6-31G(d,p)		Dihedral angles (°)	X-ray[11]	6-31G(d,p)	
		B3LYP	PBE			B3LYP	PBE
S1–C10–C9–C8	−2.1 (4)	0.65	0.72	N3–C12–S1–C10	178.8 (2)	176.13	175.56
S1–C10–C11–O3	−179.3 (2)	–179.88	–179.86	N3–C12–N2–C11	−177.1 (2)	–175.91	–175.31
S1–C10–C11–N2	2.3 (3)	–0.38	–0.37	N3–C12–N2–C13	−0.3 (4)	2.16	2.94
S1–C12–N2–C11	2.8 (3)	2.71	2.79	N3–C19–C20–C21	179.3 (3)	177.02	177.30
S1–C12–N2–C13	179.61 (18)	–179.22	–178.97	N3–C19–C24–C23	−179.8 (3)	–177.96	–178.43
S1–C12–N3–C19	−0.6 (4)	3.95	5.55	C1–C6–C7–C8	−154.6 (3)	–154.48	–156.42
O1–N1–C1–C2	33.4 (4)	21.18	18.01	C5–C6–C7–C8	26.8 (4)	28.98	27.09
O1–N1–C1–C6	−148.8 (3)	–160.41	–163.85	C6–C7–C8–C9	176.5 (2)	–177.45	–177.32
O2–N1–C1–C2	−145.6 (2)	–157.77	–160.90	C7–C8–C9–C10	−179.7 (3)	–179.61	–179.09
O2–N1–C1–C6	32.1 (4)	20.64	17.24	C8–C9–C10–C11	175.8 (2)	–179.68	–179.82
O3–C11–C10–C9	2.5 (4)	0.40	0.60	C9–C10–S1–C12	177.4 (3)	–178.75	–178.91
O3–C11–N2–C12	178.3 (2)	177.96	177.88	C10–C11–N2–C12	−3.3 (3)	–1.55	–1.62
O4–C16–C15–C14	−178.1 (3)	–179.69	–179.78	C10–C11–N2–C13	179.8 (2)	–179.64	–179.87
O4–C16–C17–C18	178.5 (3)	–179.79	–179.77	C11–N2–C13–C14	83.3 (3)	55.36	49.26
O5–C22–C21–C20	−179.3 (3)	179.69	179.56	C11–N2–C13–C18	−95.1 (3)	–123.71	–129.66
O5–C22–C23–C24	178.5 (3)	179.65	179.66	C12–S1–C10–C11	−0.7 (2)	1.56	1.59
N1–C1–C2–C3	178.8 (2)	177.36	176.89	C12–N2–C13–C14	−93.4 (3)	–122.63	–128.90
N1–C1–C6–C5	−179.8 (2)	–178.45	–177.86	C12–N2–C13–C18	88.2 (3)	58.29	52.17
N1–C1–C6–C7	1.6 (4)	4.88	5.51	C12–N3–C19–C20	81.2 (3)	54.91	47.61
N2–C11–C10–C9	−175.9 (2)	179.90	–179.91	C12–N3–C19–C24	−99.1 (3)	–129.63	–136.85
N2–C12–S1–C10	−1.1 (2)	–2.37	–2.43	C25–O4–C16–C15	170.5 (3)	–179.58	–179.66
N2–C12–N3–C19	179.3 (2)	–177.68	–176.70	C25–O4–C16–C17	−9.4 (4)	0.43	0.34
N2–C13–C14–C15	−178.6 (3)	–179.04	–178.90	C26–O5–C22–C21	−4.4 (4)	–0.47	–0.88
N2–C13–C18–C17	179.1 (2)	179.56	179.34	C26–O5–C22–C23	172.6 (3)	–179.88	179.90

Table S5: Experimental and calculated wavenumbers obtained at B3LYP and PBE functionals with 6–31g(d,p) basis set

	Exp.	B3LYP/6-31G(d,p)			PBE/6-31G(d,p)			Vibrational Assignments from B3LYP/6-31G(d,p) PED (≥(10)%)
Mode	FT-IR	Unscaled	Scaled	Int	Unscaled	scaled	Int	
162		3246.7	3120.1	1.90	3172.9	3128.5	2.61	ν_{CH} R1 (86)
161		3232.8	3106.7	5.54	3168.6	3124.2	0.60	ν_{CH} R2 (92)
160		3228.8	3102.9	3.95	3165.3	3120.9	3.86	ν_{CH} R2 (90)
159		3223.3	3097.6	9.16	3153.8	3109.7	8.87	ν_{CH} R3 (99)
158		3222.2	3096.5	6.36	3151.5	3107.4	9.12	ν_{CH} (88)
157		3219.2	3093.6	9.27	3151.1	3107	8.65	ν_{CH} R1 (84)
156		3217.1	3091.6	12.71	3150.4	3106.3	4.88	ν_{CH} R2 (91)
155		3217.0	3091.6	4.51	3149.7	3105.6	16.65	ν_{CH} R2 (90)
154		3212.0	3086.7	9.53	3146.8	3102.8	9.84	ν_{CH} R2 (89)
153		3211.9	3086.6	8.67	3142.3	3098.3	3.66	ν_{CH} R1 (92)
152		3202.3	3077.4	2.56	3136.5	3092.5	3.07	ν_{CH} R3 (93)
151		3199.2	3074.5	14.55	3130.7	3086.9	11.14	ν_{CH} R3 (94)
150		3195.2	3070.6	2.31	3128.2	3084.4	1.86	ν_{CH} R1 (91)
149		3182.2	3058.1	1.97	3107.8	3064.3	1.11	ν_{CH} (92)
148		3163.3	3039.9	5.35	3091.5	3048.2	23.86	ν_{CH} (87)
147		3151.9	3029	29.51	3090.2	3046.9	25.11	ν_{CH3} (99)
146	3008.8	3148.6	3025.8	30.94	3084	3040.8	5.18	ν_{CH3} (100)
145		3080.8	2960.7	37.90	3013.5	2971.3	33.56	ν_{CH3} (99)
144	2951.1	3074.1	2954.2	40.97	3008.8	2966.6	35.30	ν_{CH3} (100)
143	2929.7	3018.1	2900.4	65.21	2947.1	2905.8	78.39	ν_{CH3} (99)
142		3013.4	2895.9	62.60	2943.9	2902.7	74.64	ν_{CH3} (100)
141	1713.0	1795.6	1725.5	120.31	1734.9	1710.6	114.73	$\nu_{C=O}$ (79)
140	1654.2	1725.1	1657.8	865.85	1665.4	1642.1	569.07	$\nu_{C=N}$ (74)
139	1637.0	1674.0	1608.7	66.40	1624.9	1602.2	98.27	ν_{CC} R1 (68)
138	1608.0	1670.2	1605.1	65.84	1619.9	1597.3	11.78	ν_{CC} R2 (69)
137		1665.6	1600.7	23.05	1616.9	1594.3	35.92	ν_{CC} R3 (81)
136		1657.6	1592.9	133.76	1597.1	1574.8	127.83	$\nu_{C=C}$ (58)
135	1587.0	1647.6	1583.4	53.92	1591.4	1569.2	22.78	$\nu_{C=C}$ (69)
134		1636.9	1573.1	20.03	1588	1565.7	51.72	ν_{CC} R2 (63)
133	1566.1	1629.6	1566	133.88	1573.4	1551.4	116.23	$\nu_{as\ NO2}$ (58)
132		1619.8	1556.7	2.58	1571.1	1549.1	2.32	ν_{CC} R3 (66) + δ_{HCC} (10)
131	1513.7	1605.5	1542.9	60.83	1551	1529.3	99.09	ν_{CC} R1 (52) + δ_{HCC} (12)
130	1498.7	1559.5	1498.6	248.61	1510.6	1489.5	240.58	ν_{C-O} R2 (44) + δ_{CCC} (14)
129		1551.6	1491.1	208.84	1502.8	1481.8	192.01	ν_{C-O} R3 (61) + δ_{CCC} (12)
128	1461.1	1519.6	1460.3	45.52	1468.7	1448.1	50.00	δ_{HCH} (75) + τ_{HCOC} (16)
127		1519.1	1459.9	78.93	1468.2	1447.7	97.37	δ_{HCH} (75) + τ_{HCOC} (16)
126		1514.1	1455	18.83	1465.1	1444.6	35.38	δ_{HCC} (40)
125		1505.4	1446.7	5.74	1451.9	1431.6	5.93	δ_{HCH} (74) + τ_{HCOC} (25)
124		1504.4	1445.8	5.15	1451.8	1431.5	6.69	δ_{HCH} (75) + τ_{HCOC} (24)
123		1489.3	1431.3	33.08	1436.4	1416.3	7.15	δ_{HCH} (84)
122		1488.3	1430.3	27.20	1436.1	1416	43.38	δ_{HCH} (82)
121	1439.8	1481.2	1423.4	7.26	1434.1	1414	22.87	ν_{CC} R1 (26) + δ_{HCC} (48)
120		1465.9	1408.8	0.57	1428.2	1408.2	9.63	ν_{CC} R2 (47) + δ_{HCC} (18)
119		1461.3	1404.3	6.46	1426.5	1406.5	0.99	ν_{CC} R3 (48) + δ_{HCC} (24)
118	1374.4	1393.1	1338.8	208.70	1371.9	1352.7	35.30	$\nu_{s\ NO2}$ (61)
117	1345.4	1381.0	1327.2	421.52	1370.2	1351	9.54	ν_{N-C} (42) + δ_{CNC} (10)
116		1374.2	1320.6	31.66	1347	1328.1	37.48	ν_{CC} R1 (32) + δ_{HCC} (15)
115		1360.5	1307.4	157.86	1335.9	1317.2	202.29	ν_{CC} R2 (55)
114		1349.4	1296.7	31.18	1322.8	1304.2	396.79	δ_{HCC} R1 (49)
113	1295.9	1348.2	1295.6	84.99	1306.3	1288	15.72	ν_{CC} R3 (57)

112		1339.4	1287.1	62.47	1295.9	1277.8	51.55	δ_{HCC} R2 (22) + δ_{HCC} (27)
111		1338.3	1286.2	19.87	1290.2	1272.1	50.55	δ_{HCC} R2 (20) + δ_{HCC} (28)
110	1268.8	1327.7	1275.9	5.33	1280.4	1262.5	60.15	δ_{HCC} R3 (74)
109		1307.5	1256.5	42.99	1275.8	1257.9	155.30	ν_{CC} R1 (12) + δ_{HCC} (47)
108		1303.7	1252.9	219.42	1267.2	1249.5	103.94	ν_{N3C19} (41) + ν_{CC} (10)
107	1243.5	1298.2	1247.6	497.80	1264.8	1247.1	566.32	$\nu_{O\text{-}C}$ (40)
106		1289.6	1239.3	151.96	1254.4	1236.8	172.32	$\nu_{C\text{-}O}$ (33) + δ_{HCC} (20)
105		1286.2	1236	102.56	1244.4	1227	29.91	δ_{HCC} (41)
104	1183.5	1245.3	1196.7	2.05	1219.1	1202	7.16	δ_{HCC} (34)
103		1215.2	1167.8	85.81	1185.2	1168.6	135.13	ν_{NC} (10) + δ_{HCC} (18) + τ_{HCOC} (11)
102	1166.6	1212.3	1165.1	10.15	1174.4	1158	21.64	δ_{HCH} (10) + τ_{HCOC} (62)
101		1211.3	1164.1	87.97	1171.8	1155.4	10.89	τ_{HCOC} (40)
100		1201.9	1155	58.33	1168.6	1152.3	1.44	δ_{HCC} (32)
99	1148.3	1196.3	1149.7	44.02	1159.6	1143.4	110.11	δ_{HCC} (66)
98		1191.1	1144.6	77.40	1155.6	1139.4	240.57	δ_{HCC} (58)
97		1185.5	1139.3	227.32	1151.5	1135.4	26.34	δ_{HCC} (11)
96		1178.7	1132.7	0.59	1136.1	1120.2	0.62	δ_{HCH} (25) + τ_{HCOC} (74)
95		1178.5	1132.6	0.69	1135.6	1119.7	1.81	δ_{HCH} (25) + τ_{HCOC} (74)
94		1168.5	1122.9	116.57	1134.2	1118.3	84.42	ν_{NC} (30)
93		1162.7	1117.4	5.53	1127.8	1112	14.27	ν_{NC} (21) + δ_{HCC} R1 (16)
92	1100.4	1139.5	1095.1	7.87	1107	1091.5	5.81	δ_{HCC} R2 (62)
91		1133.1	1088.9	16.28	1098.9	1083.5	17.21	δ_{HCC} R3 (87)
90	1058.2	1095.7	1053	11.15	1059.4	1044.6	17.83	ν_{NC} (10) + δ_{HCC} (14) + δ_{CCC} (47)
89		1078.3	1036.2	20.56	1050.2	1035.5	17.34	$\nu_{O\text{-}CH3}$ (51)
88	1035.3	1077.1	1035.1	71.17	1047.9	1033.2	68.60	$\nu_{O\text{-}CH3}$ (73)
87		1074.6	1032.7	5.04	1046.3	1031.6	40.54	ν_{CC} (53) + δ_{HCC} (11)
86	1026.1	1069.2	1027.5	63.56	1043.6	1029	62.06	$\nu_{C10\text{-}C11}$ (30) + ν_{OC} (12)
85	1009.7	1029.2	989	1.98	997.5	983.5	1.34	δ_{CCC} R2 (67)
84		1024.8	984.9	1.16	991.8	977.9	0.67	δ_{HCC} R3(11) + δ_{CCC} (64)
83	968.2	1006.8	967.5	24.71	963.1	949.6	37.62	τ_{HCCC} (76)
82		1001.4	962.3	12.34	956.9	943.5	7.36	τ_{HCCC} (70)
81	954.2	979.1	940.9	1.92	936.7	923.5	2.01	τ_{HCCC} (87)
80	921.6	963.3	925.7	0.18	921.2	908.3	0.27	τ_{HCCC} (77) + τ_{CCCC} (20)
79		954.2	917	0.99	908.7	895.9	1.29	τ_{HCCC} (77) + τ_{CCCC} (12)
78		940.1	903.5	0.66	893.5	881	0.23	τ_{HCCC} (66) + τ_{CCCC} (15)
77		933.4	897	5.05	890.5	878	11.24	τ_{HCCC} (68)
76		933.0	896.6	3.09	885.9	873.5	2.20	τ_{HCCC} (69)
75	877.8	907.1	871.8	1.15	868.6	856.4	1.61	τ_{HCCC} (61)
74	859.0	882.5	848.1	47.11	855.9	844	29.15	δ_{NCN} (11)
73	841	876.1	842	14.48	849.3	837.4	5.51	δ_{ONO} (18) + δ_{CCC} (10)
72		871.3	837.3	6.22	843.8	832	30.55	τ_{HCCC} (75)
71	833.1	867.5	833.7	25.67	833.4	821.7	1.15	ν_{NC} (20) + τ_{HCCC} (12)
70		850.2	817.1	58.93	820.5	809	77.22	τ_{HCCC} (48)
69		847.8	814.7	17.82	815.2	803.7	30.72	τ_{HCCC} (58) + γ_{OCCC} (11)
68		846.8	813.8	38.62	811.2	799.8	29.13	δ_{ONO} (19) + τ_{HCCC} (12)
67	795.2	818.6	786.7	16.00	787.2	776.2	21.13	τ_{HCCC} (67)
66		815.6	783.8	3.13	779.2	768.3	26.76	τ_{HCCC} (75)
65		810.4	778.8	20.55	774.3	763.5	5.78	δ_{CCO} (12) + τ_{HCCC} (42)
64		802.3	771	9.62	769.5	758.7	11.68	τ_{HCCC} (51) + γ_{NCCC} (33)
63	750.3	787.7	757	8.79	765.2	754.5	7.10	$\nu_{C\text{-}O}$ (17) + δ_{CCC} (13)
62	733.5	760.8	731.1	24.12	734	723.7	5.21	τ_{HCCC} (33) + γ_{OCON} (30)
61		752.4	723.1	9.69	729.5	719.3	27.93	τ_{HCCC} (20)
60	707.9	736.1	707.4	20.47	703.3	693.5	13.76	γ_{ONCC} (71)
59	696.9	725.3	697	2.51	698.8	689	3.35	τ_{CCCC} (57)
58		715.2	687.3	9.03	689.7	680	4.84	τ_{CCCC} (22) + γ_{OCCC} (12)
57	683	710.4	682.7	12.53	683.5	673.9	11.97	τ_{CCCC} (46)
56		694.2	667.1	1.82	671.3	662	0.78	δ_{CCC} (23) + τ_{CCCC} (14)

55	647.1	665.3	639.4	11.48	646.8	637.7	10.12	δ_{CCC} (44)
54		659.3	633.6	9.19	640.1	631.1	7.42	δ_{CCC} (27)
53		650.6	625.2	2.63	627.3	618.5	1.63	δ_{CCC} (62)
52		625.1	600.7	2.51	603.6	595.2	1.15	δ_{CCC} (12)
51	591.0	611.5	587.7	6.67	593.2	584.9	7.70	ν_{SC} (10) + δ_{CNC} (11)
50		589.4	566.4	4.57	565.1	557.2	26.21	τ_{CNCN} (47) + γ_{CCCN} (20)
49	560.7	578.6	556	24.15	557.8	549.9	5.04	δ_{CNO} (19)
48		567.0	544.8	34.51	548	540.3	30.02	δ_{CNO} (17)
47		564.1	542.1	31.48	544.5	536.9	33.64	δ_{CCN} (20) + γ_{OCCC} (18)
46	531.1	541.6	520.5	22.07	520.1	512.8	22.97	τ_{HCCC} (20) + γ_{OCCC} (22)
45	514.1	534.6	513.8	2.02	515.3	508.1	3.45	τ_{CCCC} (16)
44		524.8	504.3	5.50	508.7	501.6	5.98	δ_{CCC} (15) + γ_{OCCC} (32)
43		517.4	497.2	11.51	502.5	495.4	11.37	ν_{SC} (17) + δ_{CCS} (28)
42	469.1	486.6	467.6	5.32	473.1	466.5	6.04	τ_{CCOC} (32)
41		474.5	456	6.57	457.9	451.5	4.65	τ_{CCCC} (31)
40	446.9	464.7	446.5	4.81	448.7	442.4	3.07	ν_{SC} (10) + δ_{CCN} (21)
39		450.9	433.3	4.69	436.8	430.6	3.39	δ_{CCS} (16) + τ_{CCCC} (12)
38		437.5	420.5	2.58	421.8	415.9	3.95	τ_{CCCN} (13) + τ_{CCCC} (14)
37		428.0	411.3	0.32	412.9	407.1	7.93	τ_{HCCC} (11) + τ_{CCCC} (67)
36		425.9	409.3	6.41	412.2	406.4	3.74	τ_{CCCC} (50)
35	397.6	422.4	405.9	9.16	409	403.3	1.80	δ_{CNO} (10)
34		404.6	388.8	0.36	391	385.5	1.43	ν_{NC} (14)
33		393.5	378.2	0.41	380.7	375.4	0.43	τ_{CCCC} (11) + γ_{CCCN} (10)
32		381.1	366.2	0.71	366.9	361.7	0.28	δ_{CNC} (38)
31		359.0	345	10.18	348.7	343.8	9.90	ν_{NC} (10) + δ_{CCC} (23)
30		347.7	334.2	2.55	333.8	329.2	2.62	δ_{CCS} (12) + τ_{CCCC} (17)
29		304.3	292.4	0.35	298.7	294.5	1.04	δ_{CCN} (17) + τ_{CCCC} (22)
28		299.1	287.4	5.24	292.4	288.3	1.13	δ_{CCN} (41) + τ_{CCCC} (15)
27		291.4	280.1	4.72	283.5	279.5	5.11	τ_{CCCC} (12) + τ_{HCOC} (23)
26		266.7	256.3	2.72	263.3	259.7	2.45	τ_{HCOC} (33)
25		257.1	247.1	3.68	254.7	251.1	1.36	δ_{COC} (23) + τ_{HCOC} (28)
24		249.9	240.2	0.96	248.9	245.5	2.32	δ_{COC} (37) + τ_{HCOC} (35)
23		243.9	234.4	1.71	234.5	231.3	3.56	τ_{HCOC} (21) + τ_{CCCC} (14)
22		237.0	227.7	1.76	231.3	228	5.65	τ_{HCOC} (18)
21		227.3	218.4	6.40	223.4	220.3	4.96	τ_{HCOC} (15)
20		180.8	173.7	1.24	178.2	175.7	1.60	τ_{CCCC} (36) + γ_{NCCC} (14)
19		169.6	162.9	1.83	166	163.7	2.41	τ_{CCCC} (18)
18		162.7	156.3	0.12	162.5	160.2	0.06	τ_{COCC} (10)
17		145.0	139.3	2.15	142.1	140.1	3.23	τ_{CCCC} (17)
16		133.6	128.4	3.23	134.9	133.1	2.38	τ_{CCCN} (15)
15		125.5	120.6	0.83	126.9	125.1	1.72	τ_{CCCC} (10) + γ_{CCCN} (10)
14		112.8	108.4	5.20	112.7	111.1	4.86	δ_{CCC} (18) + τ_{COCC} (14)
13		93.1	89.5	1.08	96	94.7	1.03	τ_{COCC} (44)
12		88.7	85.3	1.78	91.2	89.9	0.33	τ_{COCC} (45)
11		76.8	73.8	0.61	82.1	81	0.92	τ_{CCCN} (41)
10		64.7	62.2	0.15	63.8	62.9	0.46	τ_{ONCC} (22)
9		62.7	60.2	0.62	62.2	61.4	0.79	τ_{CNCN} (13) + τ_{CCCC} (42)
8		45.7	43.9	0.36	45.2	44.6	0.55	τ_{ONCC} (31)
7		43.9	42.2	0.41	42.3	41.7	0.81	τ_{ONCC} (22) + τ_{CNCC} (21)
6		33.8	32.5	1.24	39.8	39.2	0.85	τ_{CNCC} (68)
5		29.5	28.3	0.60	29.8	29.4	0.52	τ_{CNCC} (20) + τ_{CNCN} (33)
4		24.6	23.7	0.46	25.4	25.1	0.58	τ_{CNCC} (55)
3		18.5	17.7	1.51	18.8	18.5	1.44	δ_{CNC} (12) + τ_{CCCC} (41)
2		16.1	15.4	0.51	16.9	16.7	0.30	δ_{CNC} (30) + τ_{CCCC} (15)
1		14.7	14.1	0.84	15.6	15.4	0.85	τ_{CCCC} (57)

ν: Stretching, **δ:** Bending, **τ:** Torsion, **γ:** Out-of-plane,

Table S6: Experimental and calculated ^{1}H and ^{13}C isotropic chemical shifts (ppm) for MNTZ using the B3LYP/6–31G(d,p) level of theory

Atoms	^{1}H chemical shifts		Atoms	^{13}C chemical shifts	
	Experimental	Calculated		Experimental	Calculated
H2	8.00	8.40	C1	148.13	144.74
H3	7.43	7.39	C2	122.34	123.28
H4	7.54	7.57	C3	122.34	124.75
H5	7.64	7.67	C4	129.20	129.92
H7	7.67	7.70	C5	122.34	125.12
H8	6.71	6.95	C6	133.36	131.33
H9	7.54	7.55	C7	141.80	136.88
H14	7.35	7.42	C8	125.20	123.59
H15	6.90	7.00	C9	129.60	127.03
H17	6.90	6.80	C10	128.50	128.98
H18	7.35	7.41	C11	165.87	159.32
H20	7.04	7.03	C12	150.72	146.01
H21	6.90	6. 94	C13	122.34	124.78
H23	6.90	6.76	C14	122.34	124.08
H24	7.04	6.82	C15	114.86	112.71
H25a	3.81	3.61	C16	159.90	153.42
H25b	3.85	3.97	C17	114.57	105.44
H25c	3.81	3.61	C18	122.34	125.30
H26a	3.81	3.58	C19	135.79	136.47
H26b	3.85	3.95	C20	114.86	114.88
H26c	3.81	3.60	C21	114.57	105.48
			C22	157.20	151.14
			C23	114.86	114.03
			C24	122.34	120.43
			C25	55.65	53.01
			C26	55.57	52.85

Table S7: The thermodynamic parameters of MNTZ calculated using B3LYP and PBE functionals with 6-31g(d,p) basis set in the ground state at 298.15 K

Thermodynamic parameters	6-31G(d,p)	
	B3LYP	PBE
Zero-point vibrational energy (Kcal.mol^{-1})	266.941	259.507
Rotational constant (GHZ)	0.111	0.111
	0.048	0.048
	0.035	0.034
Rotational temperature (Kelvin)	0.005	0.005
	0.002	0.002
	0.002	0.002
Energy (Kcal.mol^{-1})		
Total	286.474	279.483
Translational	0.889	0.889
Rotational	0.889	0.889
Vibrational	284.697	277.706
Molecular capacity at constant volume (cal .mol^{-1} K^{-1})		
Total	117.661	121.162
Translational	2.981	2.981
Rotational	2.981	2.981
Vibrational	111.699	115.201
Entropy (cal.mol^{-1} K^{-1})		
Total	210.554	212.237
Translational	44.438	44.438
Rotational	38.688	38.708
Vibrational	127.428	129.091
Zero point correction (Hartree/Particle)	0.425	0.414
Thermal correction to Energy	0.457	0.445
Thermal correction to Enthalpy	0.457	0.446
Thermal correction to Gibbs Free Energy	0.357	0.346

Table S8: The calculated thermodynamic parameters of MNTZ using B3LYP/6-31g(d,p) and PBE/6-31g(d,p) levels at different temperatures

T (K)	**B3LYP/6-31G(d,p)**			**PBE/6-31G(d,p)**		
	S(J/mol.K)	Cp(J/mol.K)	ΔH(kJ/mol)	S(J/mol.K)	Cp(J/mol.K)	ΔH(kJ/mol)
100	526.08	220.18	13.92	520.47	219.42	13.73
200	724.85	368.74	43.30	718.64	370.83	43.19
298.15	900.00	517.98	86.84	894.95	521.51	87.02
300	903.21	520.73	87.80	898.18	524.27	87.99
400	1072.57	659.85	147.01	1068.61	663.65	147.56
500	1232.68	775.41	218.97	1229.54	778.92	219.9
600	1382.54	867.85	301.31	1380.01	870.87	302.57
700	1522.08	941.77	391.93	1519.97	944.27	393.46
800	1651.88	1001.66	489.20	1650.07	1003.68	490.95
900	1772.79	1050.87	591.90	1771.2	1052.5	593.84
1000	1885.70	1091.81	699.10	1884.26	1093.1	701.18